Building and Environment 298 (2026) 114662

Contents lists available at ScienceDirect

Building and Environment

journal homepage: www.elsevier.com/locate/buildenv

Data-driven climate control in autonomous electric vehicles: A machine learning approach to thermal comfort and energy use

Manuel Kipp [a,*], Ruya Wang [a], Daniel Schmeling [b], Yijie Sheng [a], Klaus Bengler [a]

[a] Technical University of Munich, Chair of Ergonomics, Boltzmannstrasse 15, Garching, 85748, Germany
[b] German Aerospace Center (DLR), Institute of Aerodynamics and Flow Technology, Bunsenstr. 10, Göttingen, 37073, Germany

HIGHLIGHTS

- 16-zone steady-state t_{eq} dataset for a Level-4 cabin at −10/ + 16/ + 28 °C.
- Forward surrogates predict 16 segmental t_{eq} values from scenario and actuator settings.
- XGBoost and Random Forest outperform a linear baseline in pooled intra-scenario validation.
- Noise and LOSO tests show strong interpolation but limited climate extrapolation.

ARTICLE INFO

Keywords:
Equivalent temperature
DIN EN ISO 14,505–2
Steady-state setpoint selection
Hybrid HVAC
Machine-learning surrogate
Energy optimization
Electric-vehicle range

ABSTRACT

Thermal management in battery-electric Level-4 cabins must balance local thermal comfort against HVAC electrical power and the resulting range penalty. This study develops and evaluates a data-driven framework for comfort-oriented and energy-aware steady-state setpoint selection for a hybrid convective–radiant HVAC concept. A vehicle-like mock-up in a climate chamber is instrumented with a 16-zone segmented thermal manikin to measure stationary local equivalent temperatures t_{eq} according to DIN EN ISO 14,505–2 under three ambient scenarios (−10 °C, +16 °C, +28 °C), two seating postures, and three air-distribution concepts. Based on the resulting steady-state dataset, forward multi-output surrogate models are trained to predict the 16 segmental t_{eq} values from boundary conditions and actuator settings, using a linear regression baseline and ensemble methods (Random Forest, XGBoost). On the pooled dataset with intra-scenario 5-fold cross-validation, XGBoost achieves a mean $R^2 = 0.978$ and a mean MAE = 0.856 K across the 16 targets, outperforming the linear baseline ($R^2 = 0.872$, MAE = 2.248 K). Scenario-level extrapolation remains limited in a leave-one-scenario-out stress test, indicating that explicit climate coverage is required for deployment beyond the represented operating space. The trained surrogate is embedded in a constrained search over the admissible actuation space to identify comfort-feasible setpoints within the Nilsson neutrality bands with minimum electrical HVAC power, computed from a convective energy balance with scenario-dependent COP and measured radiant-panel power. Validation experiments confirm near-neutral comfort in winter and summer. At +16 °C, radiant support yields only marginal comfort changes but increases electrical HVAC power from about 0.5 kW in convection-only operation to about 2.1 kW in hybrid operation, causing an estimated WLTP range penalty of roughly 15–17% in the considered reference cycle. The contribution of the present study is therefore limited to steady-state comfort-constrained setpoint selection and actuator prioritization within the measured operating space and does not extend to broadly generalizable real-time HVAC control.

1. Introduction

The automotive sector is undergoing two major transitions: highly automated driving and the electrification of the powertrain. Their combination changes the role of the vehicle cabin. In SAE Level 4 vehicles, automated driving enables Non-Driving Related Tasks (NDRTs) such as working, relaxing, or sleeping, and occupants are no longer

* Corresponding author.
Email addresses: manuel.kipp@tum.de (M. Kipp), ruya.wang@tum.de (R. Wang), daniel.schmeling@dlr.de (D. Schmeling), yijie.sheng@tum.de (Y. Sheng), bengler@tum.de (K. Bengler).

https://doi.org/10.1016/j.buildenv.2026.114662
Received 22 January 2026; Received in revised form 7 April 2026; Accepted 22 April 2026
Available online 24 April 2026

restricted to a fixed driver-oriented posture [32,56]. Instead, posture changes and more relaxed seating configurations become part of the intended use case. These changes modify local heat exchange at the body and may also affect metabolic rate depending on the activity and seating configuration [23,42]. Level 4 automation therefore increases the relevance of spatially non-uniform thermal conditions and local discomfort risks. As a result, HVAC decisions in such cabins should be justified at segment level rather than by uniform bulk-air targets alone.

This challenge is particularly important in battery-electric vehicles (BEVs). In contrast to vehicles with internal combustion engines, BEVs cannot rely on abundant waste heat for cabin conditioning. Heating, Ventilation, and Air Conditioning (HVAC) must instead draw energy directly from the traction battery [54,59]. Under cold, hot, or otherwise demanding boundary conditions, HVAC can become a major auxiliary load and can reduce driving range substantially if not managed efficiently [25,41]. This creates a direct engineering trade-off between maintaining thermally neutral conditions for relaxed occupants and minimizing electrical power consumption.

Conventional automotive HVAC control is not well suited to this setting. Standard strategies are typically centered on cabin air temperature and were developed for a largely static, driver-focused seating arrangement. Such approaches do not adequately resolve spatial gradients, stratification, and local exposures that become more relevant in flexible Level 4 interiors [3,13]. For non-uniform environments, DIN EN ISO 14,505–2 recommends the *equivalent temperature* (t_{eq}) as an integrative measure that reflects both convective and radiative heat exchange [14,38]. Segment-resolved t_{eq} therefore provides a suitable basis for objective comfort assessment and for control decisions that must satisfy local comfort constraints.

Hybrid HVAC concepts that combine convective air supply with near-field radiant elements, such as infrared (IR) panels, are a promising response to this challenge [4,30]. They can improve local comfort in cold conditions, but they also introduce additional actuators and interactions across ambient scenarios, postures, and body regions. The scientific problem is therefore not merely to combine machine learning with HVAC control. Rather, the key task is to identify which actuator combinations can satisfy segment-level comfort constraints while minimizing electrical HVAC power in a reproducible and computationally efficient way. Data-driven surrogate models are a practical option for this purpose because they can approximate the non-linear mapping from boundary conditions and actuator settings to resulting local thermal states and can therefore support fast evaluation of comfort-feasible operating points [46,57].

Against this background, the present study develops a data-driven framework for comfort-constrained and energy-aware steady-state setpoint selection in a Level 4 battery-electric cabin with a hybrid convective–radiant HVAC concept. A climate-chamber dataset is generated with a segmented 16-zone thermal manikin under three ambient scenarios (−10 °C, +16 °C, and +28 °C), two seating postures representing a more upright and a more relaxed Level 4 use case, and three air-distribution concepts. For each operating point, stationary segmental t_{eq} values are derived according to DIN EN ISO 14,505–2 and related to the Nilsson comfort zones. Forward multi-output surrogate models are then trained to predict the 16 segmental t_{eq} values from scenario descriptors and actuator settings. These models are subsequently used within a constrained search to identify comfort-feasible operating points with minimum electrical HVAC power. The study is explicitly framed as a steady-state sizing and setpoint-selection investigation within the measured operating space rather than as a transient cabin-control study. The resulting framework is positioned as a scenario-specific setpoint-selection and design-support tool whose purpose is to identify comfort-feasible operating points and actuator-prioritization rules under fixed boundary conditions, not to validate a real-time controller for arbitrary cabin dynamics. Within this scope, machine learning is employed as a compact surrogate for rapid evaluation of candidate operating points in a mixed discrete–continuous actuator space, motivated by the non-linear actuator interactions that a linear formulation cannot represent with sufficient accuracy for segment-level constraint checking.

The specific objectives and contributions of this work are as follows:

- **Dataset generation:** A reproducible steady - state dataset is established for a Level 4 cabin mock-up that links ambient scenario, seating posture, air-distribution concept, and hybrid HVAC actuation to segmented t_{eq} targets across sixteen body zones.
- **Forward surrogate modeling:** Multi-output surrogate regressors are developed to predict the 16 stationary segmental t_{eq} values from boundary conditions and actuator settings. Their performance is assessed against a linear regression baseline and complemented by robustness analyses to separate interpolation capability from extrapolation limits.
- **Energy–comfort analysis:** The comfort–power trade-off of hybrid convective–radiant operation is quantified across winter, transitional, and summer conditions, with particular attention to operating regions in which radiant support yields only marginal comfort benefits but substantial electrical power penalties.
- **Actuator prioritization rules:** Control-relevant design guidelines are derived for the prioritization of convective and radiant actuation under segment-level comfort constraints, including the identification of conditions in which lower-body radiant support is beneficial and conditions in which convection-dominated operation is preferable.

The results provide a basis for energy-aware HVAC setpoint strategies in future automated BEV cabins by combining segmented comfort constraints, steady-state surrogate evaluation, and explicit consideration of robustness and scope limits.

2. State of the art

The transition toward battery electric vehicles (BEVs) and SAE Level-4 automation requires HVAC concepts that can maintain local thermal comfort under strict energy constraints. Conventional automotive climate control was developed mainly for a single, upright driving posture and for largely uniform air-temperature targets. In contrast, Level-4 cabins enable posture changes and Non-Driving Related Tasks (NDRTs), which increase spatial non-uniformity and the relevance of actuator-selective conditioning. This section therefore reviews (i) HVAC concepts for electric and automated vehicles with emphasis on hybrid and radiant solutions, (ii) objective and subjective approaches for thermal comfort assessment in non-uniform cabins, and (iii) data-driven prediction methods that support control-oriented evaluation.

2.1. HVAC concepts in electric and automated vehicles

Early studies on BEV HVAC systems showed that directly transferring conventional air-based heating concepts to electric vehicles can cause substantial range penalties in cold ambient conditions [29]. This motivated approaches that reduce the need for bulk-air heating and instead deliver heat closer to the occupant. Conductive seat systems are a prominent example, as direct seat-based conditioning can improve thermal comfort in cool environments and reduce HVAC energy demand compared with air-only conditioning. Human-subject studies reported improved comfort in cool environments, but also pointed to the risk of local overheating at elevated setpoints [9,40].

To address local discomfort while preserving flexibility for changing postures and cabin layouts, more recent concepts combine convective airflow with additional local actuators such as conductive or radiant elements. Systems with side-panel heating or steering-wheel heating can improve post-entry comfort distribution under cold conditions [53]. Hybrid configurations that integrate radiant, convective, and conductive components have also been investigated for winter operation and can reduce heating energy while maintaining whole-body comfort, depending on the boundary conditions and control strategy [51]. Reviews and comparative studies further show that the efficiency and range impact

Table 1
Overview of HVAC concepts for electric vehicles and their main characteristics.

Reference	System focus	Main characteristics
Konz et al. [29]	Conventional convective air system	High heating load, driving-range reduction reported up to 50% under cold ambient conditions.
Brooks and Parsons [9]	Experimental conductive seat heating (subjects)	Improved overall comfort in cool environments, particularly pleasant warming of torso and thighs.
Oi et al. [40]	Seat heating (human-subject study)	Approx. 14% reduction of HVAC energy consumption, risk of local overheating and burning sensation at high setpoints.
Schmidt et al. [53]	Convective ventilation with side-panel and steering-wheel heating	More uniform thermal distribution, global comfort achieved within about 30 min after vehicle entry.
Sasaki and Sakamoto [51]	Hybrid radiant–convective–conductive heating	About 5.3% reduction in heating energy under cold winter conditions while maintaining whole-body comfort.
Kang and Lee [26]	Review of automotive HVAC systems for EVs	Review of HVAC architectures, components and control strategies for hybrid and battery EVs, focusing on energy efficiency and thermal comfort trade-offs.
Frohner et al. [19]	Novel heating concept for BEVs	Modified interior heating concept reducing traction-battery load versus conventional PTC heating while maintaining acceptable winter cabin comfort.
Al Faruque and Vatanparvar [2]	Control-oriented modeling of EV HVAC systems	System-level modeling, analysis and optimization, highlights HVAC contribution to energy use and proposes strategies accounting for battery lifetime and range constraints.
Kruppok et al. [31]	5-zone cabin model for BEV HVAC evaluation	Five-zone cabin model with validation, predicts interior temperatures and supports evaluation of HVAC energy-saving potentials across driving and climate conditions.
Gis et al. [20]	Efficiency of EV interior heating systems	Comparative analysis of EV interior heating concepts at low ambient temperatures, quantifies efficiency and shows strong technology-dependent impact on total vehicle energy consumption.
Ramsey et al. [47]	Simulation of EV range impact due to cabin heating	Powertrain-level simulation including cabin heating loads, assesses range impact of heating strategies and motivates energy-aware climate control.
Cvok et al. [12]	Optimal control of EV HVAC for range extension	Control-trajectory optimization to increase driving range while preserving passenger thermal comfort, advantages over rule-based operation.
Lahlou et al. [34]	Co-management of thermal comfort and EV driving range	Optimal management framework jointly considering comfort and range, explicitly quantifies HVAC energy–comfort trade-offs.

of cabin conditioning in BEVs depend strongly on the selected HVAC architecture and its operation [20,26,47].

Beyond component concepts, several studies have proposed control-oriented modeling and optimization frameworks to quantify energy–comfort trade-offs and derive range-aware HVAC strategies [2,12,31,34]. Table 1 summarizes representative HVAC concepts for electric vehicles and their main characteristics. Overall, the literature shows a shift from purely convective air systems toward hybrid architectures that combine convective distribution with local actuators. This trend is particularly relevant for Level-4 cabins, where posture changes and non-uniform exposures increase the value of region-specific conditioning.

2.2. Thermal comfort assessment and prediction in vehicle cabins

Thermal comfort assessment is central to the evaluation of advanced HVAC concepts. Global indices such as PMV and PPD, formalized in ISO 7730, provide an established reference for homogeneous and quasi-steady environments [15,17]. Vehicle cabins, however, are characterized by spatial gradients, directional radiation, drafts, and transient phases such as entry, warm-up, and cool-down. Under these conditions, local discomfort can dominate even when global indices appear acceptable.

For such non-uniform environments, DIN EN ISO 14,505–2 recommends the *equivalent temperature* (t_{eq}) as an objective metric that combines convective and radiative heat exchange into a single reference temperature [14]. Nilsson established comfort zones and showed how t_{eq} can be related to thermal sensation in complex environments [38]. Later work proposed linearized formulations to support rapid and control-oriented evaluation of equivalent temperature [50]. In vehicle cabins, segment-resolved t_{eq} is particularly useful because it enables local comfort constraints for body regions that are sensitive to drafts, asymmetrical radiation, and cold or warm boundary surfaces.

Objective metrics alone, however, do not fully represent occupant perception. Subjective ratings remain important for validation and interpretation, and automotive comfort studies therefore often combine climate-chamber measurements with overall and local sensation or comfort votes. Recent work has emphasized the need for harmonized procedures and robust comparability when assessing local comfort effects of air distribution and drafts [43,60]. This supports the use of segment-level objective metrics as a structured engineering basis, while also requiring a clear statement of scope and limitations when transferring manikin-based results to human occupants.

2.3. Data-driven prediction of thermal comfort

The increasing availability of sensor data and the complexity of hybrid HVAC architectures have motivated data-driven methods for comfort prediction and control-oriented evaluation. Instead of relying only on first-principles models, machine-learning approaches learn statistical relationships between boundary conditions, actuator states, and comfort-related targets from experimental or field data. In vehicle applications, these targets are often overall thermal sensation votes, comfort classes, or temperatures derived from measurements and surrogate indices.

Linear and multiple regression have been used to predict overall thermal sensation with moderate accuracy from cabin conditions [65]. Tree-based models such as Random Forest have been applied to improve predictive performance compared with empirical approaches [35]. Other studies combined several algorithms to infer seat-heating patterns or comfort classes and reported high accuracy for specific tasks and feature sets [24]. Hybrid approaches that combine CFD with machine learning further show that surrogate models can approximate thermal quantities with high accuracy while reducing computation time compared with full CFD simulations [57]. Comparative work also shows that model performance depends strongly on the available sensors, the selected targets, and the diversity of the covered boundary conditions [46,62,64].

Table 2 summarizes representative studies on data-driven comfort prediction in vehicle cabins. Most of these approaches focus on global indices, subjective votes, or a limited subset of local variables, and they are often evaluated for restricted ambient ranges, seat configurations, or actuator subsets. Their transfer to Level-4 cabins is therefore limited, because posture changes and spatial non-uniformity require segment-level constraints, while energy-aware operation requires actuator decisions that remain valid across multiple scenarios.

In summary, prior work shows that hybrid HVAC concepts and data-driven models can improve comfort and energy efficiency. However, systematic studies remain limited that (i) use segment-resolved t_{eq} as an objective local constraint metric, (ii) cover multiple ambient scenarios together with posture-dependent Level-4 use cases, and (iii) support energy-aware steady-state setpoint selection across a hybrid actuator space. The present work addresses this gap by combining segmented t_{eq}-based evaluation with forward surrogate regression models for the

Table 2
Selected studies on thermal comfort prediction in vehicle cabins.

Author	Modeling method	Comfort index	Reported accuracy
Yun et al. [65]	Linear and multiple regression	Overall Thermal Sensation (OTS)	$R^2 \approx 0.61$
Lee et al. [35]	Random Forest	Overall Thermal Sensation	Prediction accuracy improved by a factor of 2.6 compared to traditional methods
Ju et al. [24]	Decision tree, SVM and k-Nearest Neighbors	Seat-heating pattern / comfort class	Up to $R^2 = 0.96$ for pattern prediction
Warey et al. [57]	CFD + SGD regression, Random Forest, neural network	Equivalent homogeneous temperature	> 95% prediction accuracy, strong reduction in computation time versus pure CFD
Yu et al. [64]	Comparative study of ML algorithms (kNN, RF, SVM, XGBoost) with multi-sensor inputs	Individual thermal sensation vote and comfort vote	Best-performing models reach classification accuracies above 80% using reduced feature sets from low-cost sensors, demonstrating practical deployment potential.
Xu et al. [62]	Multiple regression models using local skin and breathing air temperatures in a vehicle cabin	Overall thermal sensation (OTS) and overall thermal comfort (OTC)	Prediction models for OTS and OTC achieve $R^2 = 0.77$ and $R^2 = 0.51$, respectively, identify chest skin and breathing air temperature as key predictors for intelligent cabin control.
Qavidel Fard et al. [46]	Review and benchmarking of ANN, SVM and tree-based comfort models	Various indices (PMV, TSV, preference, comfort vote)	Synthesizes reported accuracies typically between 70–90% across algorithms and datasets, highlights strengths, limitations and data requirements of individual methods.

prediction of stationary local thermal states and by explicitly distinguishing strong interpolation performance within the measured design space from limited scenario-level extrapolation.

3. Fundamentals

This section summarizes only the physical and methodological fundamentals that are directly required for the present study. First, the dominant heat-transfer paths between occupant and cabin are outlined to motivate the combined use of convective and radiative conditioning. Second, the electrical HVAC power demand and its effect on WLTP range are introduced. Third, local thermal comfort in non-uniform cabins is described by segmental equivalent temperature and the Nilsson comfort zones according to DIN EN ISO 14,505–2. Finally, the learning task is stated in its reduced form to define the forward surrogate used later in the Methods section.

3.1. Heat transfer between occupants and the cabin environment

Heat exchange between an occupant and the surrounding cabin is governed by conduction, convection, and long-wave thermal radiation [10,44]. In the present HVAC concept, the relevant active actuation paths are forced convection through the air-distribution system and near-field radiation from infrared panels. Conductive heat transfer is not used as an active control path in the investigated configuration. For one body segment, the sensible heat exchange can therefore be written as

$$\dot{Q}_{\mathrm{sens}} = \dot{Q}_{\mathrm{conv}} + \dot{Q}_{\mathrm{rad}}, \tag{1}$$

where $\dot{Q}_{\mathrm{conv}}$ depends mainly on local air temperature and air motion, and $\dot{Q}_{\mathrm{rad}}$ depends on the radiative exchange with surrounding surfaces and local radiant sources [17,38]. In vehicle cabins, radiative asymmetries and local airflow effects can differ strongly between body regions. This motivates segment-resolved comfort metrics and actuator-selective conditioning.

3.2. Electrical HVAC power demand and impact on WLTP range

In battery electric vehicles, HVAC energy is drawn from the traction battery and therefore contributes directly to range reduction. The electrical power demand depends on the required thermal load, the efficiency of the heating or cooling process, and additional auxiliary loads. For the heat-pump-based actuation path, the coefficient of performance (COP) is defined as

$$\mathrm{COP} = \frac{\dot{Q}_{\mathrm{clim}}}{P_{\mathrm{el,HP}}}, \tag{2}$$

where $\dot{Q}_{\mathrm{clim}}$ is the delivered heating or cooling capacity and $P_{\mathrm{el,HP}}$ is the corresponding electrical input power [52]. Lower ambient temperatures typically reduce the COP and therefore increase the electrical power demand for a given thermal output.

The total electrical HVAC power is modeled as

$$P_{\mathrm{el,HVAC}} = P_{\mathrm{el,HP}} + P_{\mathrm{el,blower}} + P_{\mathrm{el,aux}}, \tag{3}$$

where $P_{\mathrm{el,blower}}$ represents the blower power for convective air distribution and $P_{\mathrm{el,aux}}$ aggregates additional electrical loads. In the present hybrid concept, the radiant panels are treated as electrical auxiliary loads and are therefore included directly in $P_{\mathrm{el,aux}}$.

To estimate the range impact, a simplified WLTP-based engineering model is used following [5,61]. For a representative vehicle with battery capacity E_{bat}, average traction power P_{drive} over the WLTP cycle, cycle distance d_{WLTP}, and cycle duration t_{WLTP}, the achievable range is approximated as

$$R_{\mathrm{WLTP}} = \frac{E_{\mathrm{bat}}}{P_{\mathrm{drive}} + P_{\mathrm{el,HVAC}}} \frac{d_{\mathrm{WLTP}}}{t_{\mathrm{WLTP}}}. \tag{4}$$

This formulation is used to quantify the relative impact of HVAC operation on range. It is not intended to replace a full vehicle-energy simulation. For the scenario-specific calculations, COP values of 2.3, 2.7, and 3.5 are assumed for −10 °C, +16 °C, and +28 °C, respectively, consistent with reported temperature-dependent performance trends in the literature [36,37,55].

3.3. Local thermal comfort in non-uniform vehicle environments

Highly automated cabins with flexible seating layouts and hybrid HVAC actuation are characterized by spatial non-uniformity in temperature, radiation, and airflow. Under such conditions, global comfort indices that assume uniform environments have limited diagnostic value for local discomfort mechanisms.

3.3.1. Equivalent temperature as an objective local metric

DIN EN ISO 14,505–2 recommends the *equivalent temperature* t_{eq} as an objective metric for non-uniform vehicle environments [14]. The concept combines convective and radiative heat exchange into a single reference temperature that produces the same sensible heat loss in a standardized isothermal environment [38]. Segment-resolved t_{eq} values can be measured with a segmented thermal manikin and are therefore well suited for local comfort assessment in cabins with directional airflow and radiative asymmetries.

3.3.2. Nilsson comfort zones and constraint formulation

Nilsson and Holmér developed comfort-zone diagrams that relate segmental equivalent temperature to local thermal sensation and were later incorporated into DIN EN ISO 14,505–2 [14,39]. For each body segment, neutral reference values and acceptable comfort bands can be derived from the relationship between t_{eq} and local sensation votes. In the present work, these segment-specific neutral bands are used as local comfort constraints. The segmented thermal manikin measures t_{eq} for the corresponding sixteen body zones, and the surrogate models predict the 16 segmental t_{eq} values as a function of ambient scenario and HVAC settings. During the setpoint search, all predicted segmental t_{eq} values must remain within the Nilsson neutral ranges while the electrical HVAC power $P_{\mathrm{el,HVAC}}$ from Section 3.2 is minimized.

3.4. Learning task used in this work

The data-driven component of this study is restricted to a supervised forward surrogate for steady-state conditions. Let $\mathbf{x} \in \mathbb{R}^p$ denote the feature vector containing scenario descriptors and actuator settings, and let $\mathbf{y} \in \mathbb{R}^q$ denote the multi-target output vector containing the 16 segmental equivalent temperatures. The learning task is to approximate the mapping

$$\hat{\mathbf{y}} = f(\mathbf{x}), \tag{5}$$

so that stationary local thermal states can be predicted from candidate operating points. The resulting surrogate is then used for fast evaluation within a comfort-constrained search. Detailed preprocessing, model training, baseline comparison, and robustness evaluation are reported in Section 5.6.

4. Objectives

The aim of this study is to develop and evaluate a data-driven framework for comfort-constrained and energy-aware steady-state setpoint selection in highly automated battery-electric vehicles equipped with a hybrid convective–radiant HVAC system. The work builds on previous winter-focused research at −10 °C and extends it to multiple ambient conditions, a broader hybrid actuator space, and a forward surrogate workflow that is explicitly formulated for stationary Level-4 cabin scenarios. The focus is therefore not on transient online control, but on identifying actuator combinations that satisfy segment-level comfort constraints while minimizing electrical HVAC power within the measured design space.

Building on segmented thermal-manikin measurements and controlled climate-chamber experiments, the study pursues the following specific objectives:

1. **Generate a reproducible multi-scenario dataset for segment-level comfort and HVAC power.** Establish an experimental database that links ambient conditions (−10 °C, +16 °C, +28 °C), two seating postures representing a more upright and a more relaxed Level-4 use case, air-distribution concepts, and hybrid HVAC actuation to local equivalent temperature t_{eq} across sixteen body segments and to the associated electrical HVAC power demand.
2. **Develop and evaluate forward surrogate models for stationary segmental t_{eq} prediction.** Train multi-output regression models that map scenario descriptors and actuator settings to the 16 stationary segmental t_{eq} values. Evaluate their performance against a linear regression baseline using pooled intra-scenario cross-validation, and assess robustness by controlled input-noise perturbations and leave-one-scenario-out testing to distinguish interpolation capability from scenario-level extrapolation limits.
3. **Quantify the energy–comfort trade-off of hybrid convective–radiant operation across climates.** Analyze how operating strategies at −10 °C, +16 °C, and +28 °C affect both segment-level thermal neutrality and electrical HVAC power. Particular emphasis is placed on identifying operating regions in which radiant support is beneficial and regions where it becomes energetically unfavorable despite only marginal comfort gains.
4. **Derive actuator prioritization rules for Level-4 cabin conditioning.** Translate the surrogate-based setpoint search into practical guidelines for prioritizing convective and radiant actuation, including the identification of scenario-dependent operating regions, preferred air-distribution modes, suitable mass-flow levels, and the selective use of radiant support, especially for lower-body comfort in cold conditions.

5. Method

Thermal comfort was evaluated in a climate-controlled chamber using a vehicle-like mock-up equipped with a segmented thermal manikin. Local equivalent temperatures were measured for sixteen body regions under three ambient scenarios, namely winter (−10 °C), transitional (+16 °C), and summer (+28 °C). HVAC settings, including blower speed, outlet-air temperature, air-distribution concept, and radiant-panel temperatures, were varied systematically. All data used for the data-driven framework correspond to stationary operating points. The study is therefore interpreted as a steady-state sizing and setpoint-selection investigation within the measured operating space rather than as transient cabin control.

The following subsections describe the experimental set-up, the ambient scenarios and operating concepts, the parameter matrix, the steady-state extraction procedure, and the forward surrogate modeling workflow used for comfort-constrained and energy-aware setpoint selection.

5.1. Experimental set-up and sensing concept

The experimental set-up extends the climate bench and hybrid HVAC concept introduced in [28] to a broader operating space with three ambient scenarios and two Level-4 seating postures. The subsections below describe the climatic test environment, the hybrid convective–radiant HVAC system, the seating configurations, and the segmented thermal manikin. Together, these elements provide a reproducible platform for generating steady-state equivalent-temperature data and corresponding HVAC power measurements.

5.1.1. Climate chamber and HVAC mock-up

All measurements were conducted in the climate chamber of the Chair of Ergonomics at the Technical University of Munich. The test bench consists of the front half of a B-segment vehicle mock-up integrated into a climate-controlled chamber that maintains a constant ambient temperature. The HVAC system supplies conditioned air by mixing heated and cooled air streams and distributes it into the cabin through nine symmetrically arranged outlets that are geometrically inspired by the Audi Skysphere concept [28]. The outlet layout includes dashboard outlets, footwell nozzles, and additional ports that support distinct air-distribution concepts and localized exposure of the occupant.

A panel-based infrared (IR) heating system is integrated into side panels and the floor region to realize hybrid convective–radiant operation as described in [27,28]. The geometry of the mock-up and the enclosure of the climate chamber enable repeatable air-distribution concepts and localized radiant exposure while shielding external disturbances, as shown in Fig. 1.

Table 3 summarizes the measurement channels used in the present study, their location in the climate-bench setup, their signal source or sensor type where relevant, and their role in the subsequent steady-state analysis. Additional implementation details of the previously established climate bench are reported in [28].

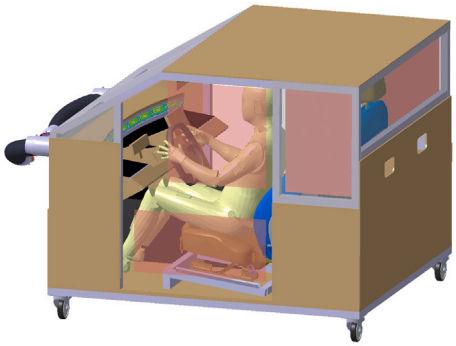

Fig. 1. Seat cabin with dashboard and footwell outlets and distributed infrared panels integrated into a climate chamber.

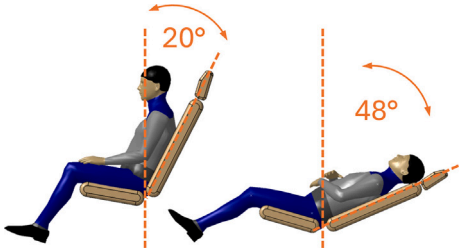

Fig. 2. Driver (left) and relax (right) seating configurations with climate dummy and respective backrest angles [28].

5.1.2. Seating configurations

To represent typical use cases in highly automated vehicles, two seating configurations were used, namely a more upright *driver* posture with a backrest angle of 20° and a more reclined *relax* posture with a backrest angle of 48°, as shown in Fig. 2. Both configurations are based on the recommendations of Yang et al. [63] for realistic driver-oriented and relaxation-oriented seating positions in future automated vehicles. They differ mainly in backrest angle and pelvis position. The climate dummy is mounted rigidly in each posture and is not repositioned during an individual experiment.

5.1.3. Segmented thermal manikin and equivalent temperature

Thermal comfort evaluation is based on the equivalent temperature t_{eq} according to DIN EN ISO 14,505–2. A segmented thermal dummy with sixteen body zones is used to measure local t_{eq} values under stationary conditions. Each segment comprises an internal heating element and surface temperature sensing. The control system adjusts the segmental surface temperatures such that the sensible heat loss matches that of a standardized isothermal reference environment, which allows the equivalent temperature to be inferred from the segment energy balance [14,39].

Fig. 3 shows the segmentation layout. The sixteen segments correspond to the body regions used in the Nilsson comfort framework and therefore enable direct mapping between measured t_{eq} values and local neutral comfort zones [39]. The climate dummy represents a 50th-percentile male occupant and follows the segmented layout described in [48]. The resulting 16-segment t_{eq} distribution forms the target space for all subsequent steady-state analyses and surrogate models.

5.2. Climate scenarios and operating concepts

The HVAC operating space is investigated under three ambient scenarios that represent typical European operating conditions for battery-electric vehicles:

- **Winter:** $T_{amb} = -10$ °C, representing severe cold conditions.
- **Transitional:** $T_{amb} = +16$ °C, representing moderate conditions between heating- and cooling-dominated operation.
- **Summer:** $T_{amb} = +28$ °C, representing warm cooling conditions.

Fig. 3 illustrates the segmented climate dummy used for comfort evaluation. In all scenarios, comfort assessment follows DIN EN ISO 14,505–2. For winter and transitional conditions, the winter comfort diagram is applied. For summer conditions, the summer comfort diagram is used. Segmental t_{eq} values are evaluated against the corresponding Nilsson neutrality bands [14].

Table 3
Instrumentation overview of the climate-bench setup used for the present study. The table summarizes the measurement channels included in the steady-state dataset, their location, the signal source or sensor type where relevant, and their role in the subsequent analysis.

Measurement channel	Location in the setup	Signal source / sensor type	Role in the analysis
Segmental equivalent temperature t_{eq} (16 zones)	Segmented thermal manikin; sixteen body regions	Segmented manikin measurement system with internal segment heating and surface temperature sensing	Primary comfort target; mapped to Nilsson neutral comfort zones and used as regression output.
Segment surface-temperature sensing and internal segment heating	Inside each manikin segment	Internal manikin control and surface-temperature sensing	Enables equivalent-temperature determination according to DIN EN ISO 14,505–2 under steady-state conditions.
Cabin air temperature	Climate chamber / cabin interior measurement positions	Type-K thermocouples	Characterization of ambient and cabin thermal boundary conditions during each operating point.
Cabin air humidity	Climate chamber / cabin interior measurement positions	Humidity measurement channel of the climate-bench instrumentation	Characterization of psychrometric boundary conditions during each operating point.
Outlet-air temperature setpoint / measured outlet conditions	HVAC air-distribution path and cabin outlets	HVAC setpoint signal and temperature measurement in the air path	Continuous model input; defines convective actuation intensity.
Fan-speed signal and mass-flow proxy	Air-handling unit / blower system	Blower-speed signal; mass-flow proxy derived from the blower setting and bench characterization	Continuous model input representing supplied airflow intensity.
Air-distribution concept / outlet-angle configuration	Dashboard and footwell outlet arrangement	Discrete outlet-angle configuration of the selected flow concept	Categorical model input defining the selected flow concept (baseline, direct, enveloping).
Radiant-panel temperature setpoints / measured panel temperatures	Side panels, center-console region, and footwell region	Panel-temperature signals of the radiant heating system	Continuous model input for radiant actuation and basis for electrical panel-power estimation.
Electrical power channels	Convective HVAC path and radiant panels	Electrical power measurements of convective and radiant subsystems	Used for the energy assessment and WLTP-based range comparison.

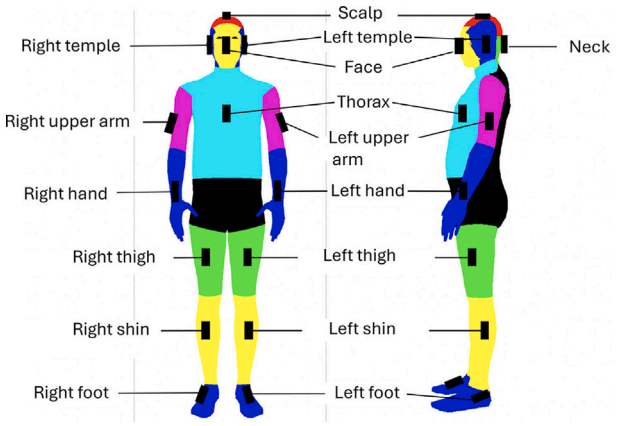

Fig. 3. Segmented climate dummy with sixteen body zones and associated equivalent temperature sensors, adapted from Kipp et al. [27].

The hybrid HVAC architecture combines

- forced convection via nine air outlets at head, mid, and foot level,
- long-wave radiant heating via heating elements integrated into side panels and the floor region,
- adjustable blower speed as a proxy for supplied mass flow.

Three air-distribution concepts are considered for each seating configuration, as shown in Fig. 4. From a control perspective, they correspond to a *baseline* concept, a *direct* concept with focused jets toward selected body areas, and an *enveloping* concept with more tangential surrounding flow. The corresponding outlet angles are derived from a previous outlet-angle system study [28] and differ between heating- and cooling-dominated scenarios to account for buoyancy effects.

For each combination of ambient scenario, posture, and air-distribution concept, the system is operated until steady-state conditions are reached. Equivalent-temperature profiles and electrical power are recorded. Electrical power is measured separately for the radiant elements and the convective path and is subsequently aggregated to total HVAC power.

5.3. Parameter matrix and operating points

The full parameter matrix follows a factorial structure that combines ambient scenario, seating position, air-distribution concept, and HVAC actuation variables. Each operating point corresponds to one climate-chamber run of approximately 60 minutes and yields one steady-state record of sixteen segmental equivalent temperatures and the associated electrical HVAC power.

The matrix covers all combinations of

- seating position: driver vs. relax,
- air-distribution concept: baseline, direct, enveloping,
- outlet air temperature T_{out},
- radiant panel temperature levels T_{IR}, where applicable,
- blower speed n_{fan} and the associated mass-flow proxy.

Across all three ambient scenarios, this factorial design yields a total of 630 operating points. These comprise 360 winter points, 180 transitional points, and 90 summer points. The transitional dataset contains both convection-only and restricted hybrid operation. This explicit count is important because the learning task is evaluated on a structured but still finite steady-state design space rather than on a continuously sampled operating domain.

In addition to the scalar setpoints, the air-distribution concepts are defined by fixed horizontal and vertical outlet angles on the driver side, with passenger-side outlets adjusted mirror-symmetrically. The baseline concept represents a conventional flow with moderate deflection and without strong jet impingement on the occupant. The direct concept aims jets at selected body regions. The enveloping concept redirects the flow away from the body to create a more diffuse surrounding airstream. The concept definitions and outlet angles follow previous investigations [28].

Before fitting non-linear surrogate models, the stationary dataset is further explored with multivariate methods to identify dominant couplings between actuator settings and segmental equivalent temperatures and to verify the internal consistency of the measured operating space.

5.4. Data acquisition and steady-state extraction

All training and validation data are obtained from systematic climate-chamber measurements with the segmented climate dummy under the three ambient scenarios defined in Section 5.2. For each parameter combination in the matrix, the cabin is driven to a quasi-steady operating point and all relevant thermal and HVAC variables are recorded. The following subsections describe the measurement protocol and the steady-state extraction procedure used to derive one feature-target pair per operating point.

5.4.1. Measurement protocol

For each parameter combination, a dedicated experiment is conducted. After setting the desired ambient temperature in the climate chamber and stabilizing the HVAC system, the corresponding outlet angles, outlet-air temperature, radiant-panel temperature, and fan speed are applied via the system interface. The configuration is then maintained for approximately 60 minutes to allow the climate dummy and the cabin air to approach thermal equilibrium.

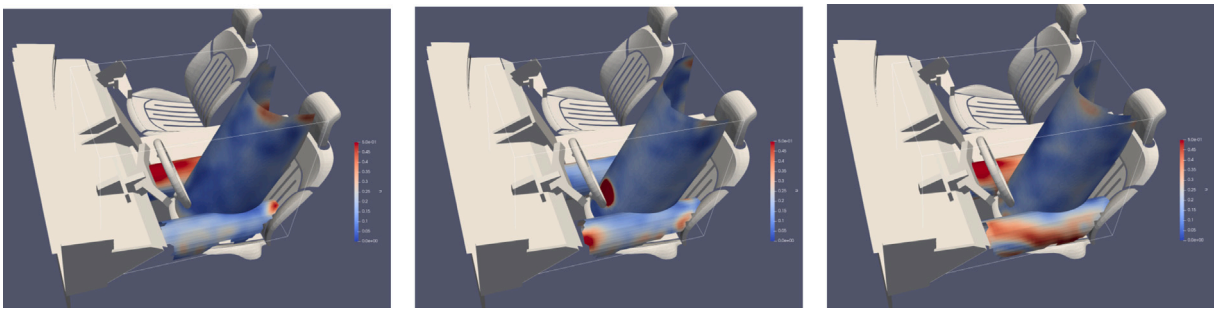

(a) Baseline (b) Direct (c) Enveloping

Fig. 4. Local velocity magnitudes visualized at simplified torso and upper-leg positions for the air-distribution concepts used across the ambient scenarios and seating postures. (a) Baseline concept combining direct and indirect flow paths, (b) direct concept with concentrated jets toward selected body areas, and (c) enveloping concept with flow guided around the occupied zone. Flow patterns are visualized using an optically tracked 3D ultrasonic velocity and temperature probe.

Following Rolle et al. and Küchle [33,48], this duration is chosen to ensure quasi-steady conditions for all body segments. Equivalent temperatures, cabin air temperatures, humidity, and HVAC operating variables are recorded continuously throughout the run and stored in a centralized data-logging system for subsequent processing.

5.4.2. Preprocessing and determination of stationary equivalent temperatures

After data collection, all time series are processed in a uniform manner to obtain one representative steady-state value per measured variable and operating point. The goal is to derive, for each run, a target vector $\mathbf{y}$ containing the sixteen stationary segmental equivalent temperatures and a corresponding feature vector $\mathbf{x}$ containing the ambient and actuator settings.

Stationarity criteria

A state is classified as stationary when all of the following conditions are satisfied:

1. The equivalent-temperature time series is filtered to suppress high-frequency fluctuations outside the relevant comfort bandwidth,
2. Within a sliding window of 20 minutes, the variation of the filtered t_{eq} signal remains below 1.5 K,
3. The representative steady-state value is computed as the arithmetic mean over the last 10 minutes of the identified stationary interval.

These criteria are applied consistently to all body segments and all runs. The resulting means define the stationary equivalent temperatures t_{eq} for the sixteen body segments and the stationary values of the corresponding HVAC inputs. Collecting these means across all channels yields one feature-target pair $(\mathbf{x}, \mathbf{y})$ per operating point.

5.5. Data pre-analysis

Before fitting the surrogate models, the stationary dataset is examined using linear multivariate analysis and visual comfort maps. The aim is to identify dominant actuator-response couplings, verify physical plausibility, and support the later definition of feasible search regions.

5.5.1. PLS-based exploration of actuator-response coupling

Partial least squares (PLS) regression is applied separately to the winter, transitional, and summer datasets. For each scenario, the predictor matrix $\mathbf{X}$ contains centered and scaled actuator and boundary-condition variables, while the response matrix $\mathbf{Y}$ comprises the sixteen stationary segmental equivalent temperatures [1,21].

Across all scenarios, the first latent component is associated with the overall heating or cooling intensity. In heating-dominated data, this component is driven mainly by outlet-air temperature and radiant-panel temperature. In cooling-dominated data, outlet-air temperature and mass flow dominate. Secondary components differentiate between upper and lower body regions and between air-distribution concepts. These patterns are used as a plausibility check and to support the subsequent forward modeling of segmental t_{eq}.

5.5.2. 3D ISO comfort diagrams

To visualize the joint effect of convective and radiant actuation on local comfort, 3D ISO comfort diagrams are generated based on the equivalent-temperature concept of DIN EN ISO 14,505–2 [14] and are oriented toward the 2D representation in [48]. For selected body regions and scenarios, the stationary dataset is interpolated on regular grids in the (T_{out}, T_{IR}) and (T_{out}, n_{fan}) planes. The resulting surfaces in Fig. 5 represent the measured equivalent temperature t_{eq} as a function of two control variables.

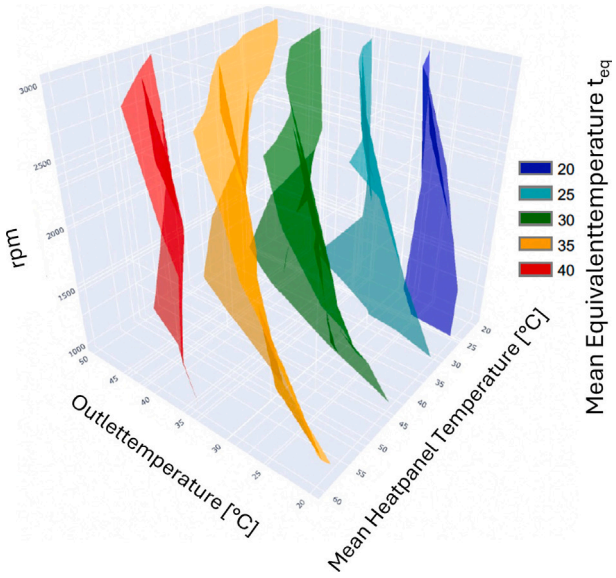

Fig. 5. 3D ISO comfort diagram for a selected body region, constructed from the stationary dataset using the DIN EN ISO 14,505–2 equivalent temperature concept.

These comfort maps provide a compact visualization of the measured operating space and its relation to the Nilsson comfort zones. They also support the definition of physically meaningful bounds for the later setpoint search.

5.6. Forward surrogate modeling and setpoint selection

Based on the stationary dataset, a data-driven surrogate model is developed to provide fast predictions of segmental equivalent temperatures for candidate actuator combinations within the measured operating space. The learning task is formulated as a forward model,

$$f : \mathbf{x} \mapsto \hat{\mathbf{y}}, \tag{6}$$

where $\mathbf{x}$ contains scenario descriptors and actuator settings, and $\hat{\mathbf{y}} \in \mathbb{R}^{16}$ contains the predicted stationary segmental t_{eq} values. The trained surrogate is then embedded in a constrained search that checks segment-wise Nilsson comfort bounds and selects minimum-power operating points.

5.6.1. Problem formulation and control-oriented use

For a fixed ambient scenario and seating configuration, the goal is to identify actuator settings that keep all predicted segmental equivalent temperatures within the Nilsson neutrality bands while minimizing total electrical HVAC power. A candidate operating point $\mathbf{x}$ is feasible if

$$t_{eq,j}^{min} \le \hat{t}_{eq,j}(\mathbf{x}) \le t_{eq,j}^{max} \qquad \forall j \in \{1, \dots, 16\}, \tag{7}$$

with $t_{eq,j}^{min}$ and $t_{eq,j}^{max}$ taken from the scenario-consistent Nilsson comfort diagram [14]. Among all feasible candidates, the operating point with minimum estimated electrical HVAC power is selected. Because all measurements and targets are stationary, this procedure is interpreted as steady-state setpoint selection within the measured design space rather than transient trajectory control.

5.6.2. Feature definition and preprocessing

For each operating point, the steady-state extraction described above yields a feature vector $\mathbf{x}$ and a target vector $\mathbf{y}$:

- **Categorical inputs:** ambient scenario, seating position, air-distribution concept.

Table 4
Discrete parameter levels and operating modes for the three ambient scenarios. The full dataset is obtained by combining all listed levels with both seating positions and all three air-distribution concepts (baseline, direct, enveloping).

Scenario	Operation mode	Outlet air temperature T_{out}	Radiant panel temperature T_{IR}	Fan speed n_{fan}
Winter −10 °C	Hybrid convection + IR heating	20, 30, 40, 50 °C	20, 30, 40, 50, 60 °C	1000, 2000, 3000 rpm
Transitional +16 °C	Convection-only (cooling / mild heating)	10–30 °C in 5 °C steps	off	1000, 2000, 3000 rpm
Transitional +16 °C	Hybrid convection + IR heating (restricted range)	10–30 °C in 5 °C steps	20, 25, 30 °C	1800 rpm
Summer +28 °C	Convection-only cooling	10–30 °C in 5 °C steps	off	1000, 2000, 3000 rpm

Table 5
Retained hyperparameters of the forward surrogate models used for stationary prediction of the sixteen segmental t_{eq} values. Parameters not listed here were kept at their library defaults.

Model	Retained settings
Linear regression baseline	Multi-output linear regression within the shared preprocessing pipeline; no tuned model-specific hyperparameters.
Random Forest	$n_{estimators}$ = 100, max_features = `sqrt`; implemented as one regressor per segment within the shared preprocessing pipeline. All remaining parameters were kept at their library defaults.
XGBoost	$n_{estimators}$ = 150, max_depth = 3, γ = 0.0; implemented as one regressor per segment within the shared preprocessing pipeline. All remaining parameters were kept at their library defaults.

- **Continuous inputs:** outlet-air temperature setpoint, fan-speed setpoint, radiant-heating setpoints, and a mass-flow proxy derived from the blower setting and validated by measurements.
- **Targets:** the sixteen stationary segmental t_{eq} values.

Categorical variables are one-hot encoded to avoid unintended ordinal assumptions. Continuous variables are standardized to zero mean and unit variance. All preprocessing steps are implemented within a single pipeline that is fitted on the training folds only. This avoids information leakage and ensures directly comparable model evaluation across baseline and ensemble methods.

5.6.3. Model classes and hyperparameters

Three regression model families are evaluated for the forward surrogate:

- **Linear regression baseline:** transparent reference model for parsimony.
- **Random Forest (RF):** tree ensemble for non-linear relationships with strong robustness to input noise [8].
- **XGBoost:** gradient-boosted trees for structured non-linear actuator interactions [11].

Multi-output prediction is implemented using one regressor per segment under a shared preprocessing pipeline. The retained hyperparameters of the reported forward surrogate models are summarized in Table 5 to support reproducibility.

5.6.4. Training, validation, baselines, and robustness tests

The main interpolation performance is evaluated by 5-fold cross-validation on the pooled dataset. The same folds and preprocessing logic are used for all model classes. Prediction accuracy is quantified with the coefficient of determination R^2 and the mean absolute error (MAE). For one target y and N samples,

$$\mathrm{MAE} = \frac{1}{N}\sum_{i=1}^{N}\left|y_i - \hat{y}_i\right|, \qquad R^2 = 1 - \frac{\sum_{i=1}^{N}(y_i - \hat{y}_i)^2}{\sum_{i=1}^{N}(y_i - \bar{y})^2}, \tag{8}$$

where $\bar{y}$ denotes the sample mean. Metrics are computed per segment and aggregated across folds, scenarios, and body segments.

To address parsimony and robustness concerns, three complementary evaluations are conducted:

1. **Baseline comparison:** a linear regression baseline is trained and evaluated under the same cross-validation protocol.
2. **Input-noise sensitivity:** zero-mean Gaussian noise with $\sigma = 1$ K is injected into the continuous input variables in the original feature space before preprocessing. Multiple Monte-Carlo realizations are evaluated and the resulting increase in MAE is used as a robustness indicator.
3. **Leave-one-scenario-out (LOSO) stress test:** one ambient scenario is withheld entirely for testing while the models are trained on the remaining scenarios. This probes scenario-level extrapolation beyond the represented operating space.

The main pooled intra-scenario cross-validation results of the retained forward surrogate models are reported in Section 6.3 and Table 9.

5.6.5. Control-oriented selection

For a given ambient scenario and seating configuration, an exhaustive search over the admissible actuator space is performed using the trained forward surrogate models. The search enumerates all combinations of T_{out}, radiant-temperature levels, and n_{fan} within the bounds of the parameter matrix shown in Table 4 for each air-distribution concept. For each candidate, the surrogate predicts the sixteen segmental equivalent temperatures, which are then checked against the segment-wise Nilsson neutrality bands.

Candidates are classified as feasible if all segmental equivalent temperatures lie within their respective comfort bands. For feasible candidates, the electrical HVAC power is evaluated using the power model in Section 5.7, and the minimum-power solution is selected. This yields comfort-compliant stationary operating points that are optimized for energy efficiency within the measured operating space of the hybrid convective–radiant HVAC concept.

5.7. HVAC power model and COP

To assess the energy impact of comfort-compliant HVAC settings, the electrical power consumption of the hybrid convective–radiant system is computed for each stationary operating point. The calculation combines a convective energy balance for the air-side heating or cooling load with empirically identified power–temperature relationships for the radiant panels and scenario-specific efficiency assumptions for the heat-pump-based path.

Fig. 6 summarizes the considered energy flows. The control volume encloses the air-handling unit and the cabin air domain. Convective heating or cooling is represented by the enthalpy difference between inlet and outlet air streams. Radiant heating is represented by the electrical power of the individual panels.

5.7.1. Convective heating and cooling power

The starting point is the steady-state energy balance for a control volume with inflowing and outflowing air streams,

$$\frac{\mathrm{d}E}{\mathrm{d}t} = \sum_{\mathrm{in}} \dot{m}_i h_i - \sum_{\mathrm{out}} \dot{m}_j h_j + \dot{Q} + \dot{W}, \tag{9}$$

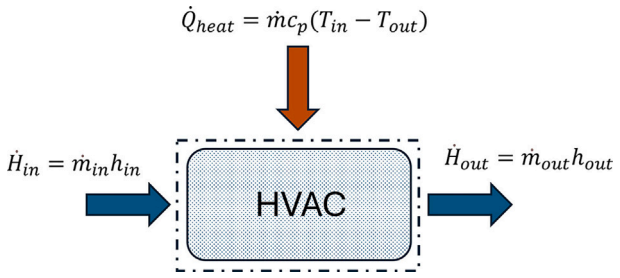

Fig. 6. Schematic energy balance around the hybrid HVAC system. Convective loads are determined from mass flow rate and moist-air enthalpy difference between inlet and outlet, while radiant loads are supplied by electrically heated panels. The heat pump or electric heater provides the required thermal power at a given coefficient of performance (COP).

where E is the total energy within the control volume, $\dot{m}$ is the air mass flow rate, and h is the specific enthalpy of moist air. Under stationary conditions and neglecting shaft work as well as kinetic and potential contributions, the net thermal load is obtained from the enthalpy-flow difference.

The specific enthalpy of moist air is computed as

$$h(T,\varphi) = c_{p,\mathrm{air}}\,T + w(T,\varphi)\left(c_{p,\mathrm{vap}}\,T + h_{\mathrm{vap}}\right), \tag{10}$$

where T is air temperature, φ is relative humidity, $c_{p,\mathrm{air}}$ and $c_{p,\mathrm{vap}}$ are the specific heat capacities of dry air and water vapor, h_{vap} is the latent heat of vaporization, and $w(T,\varphi)$ is the humidity ratio.

For cooling operation, the air-side cooling load is evaluated from the moist-air enthalpy difference between inlet and outlet conditions,

$$\dot{Q}_{\mathrm{cool}} = \left|\dot{m}_{\mathrm{air}}\left(h_{\mathrm{out}} - h_{\mathrm{in}}\right)\right|, \tag{11}$$

where $\dot{m}_{\mathrm{air}}$ is the mean supply-air mass flow rate.

For heating operation, the convective heating load is evaluated from the temperature rise across the heater heat exchanger,

$$\dot{Q}_{\mathrm{heat}} = \dot{m}_{\mathrm{air}}\,c_{p,\mathrm{air}}\left(T_{\mathrm{out,HTX}} - T_{\mathrm{in,HTX}}\right). \tag{12}$$

These expressions provide the net convective heating or cooling load for each stationary operating point.

5.7.2. Electrical power of radiant heating panels

The radiant component of the HVAC system is implemented via multiple electrically heated panels integrated into interior surfaces. For the present climate-bench setup, the electrical power required to maintain a panel surface temperature setpoint T_i is approximated by an empirical linear model,

$$P_{\mathrm{el,panel},i}(T_i) = \beta_{0,i} + \beta_{1,i}\,T_i, \tag{13}$$

where $\beta_{0,i}$ and $\beta_{1,i}$ are obtained from dedicated current–voltage measurements under fixed boundary conditions [7,33]. The resulting coefficients are listed in Table 6.

For each stationary operating point, the electrical power of all active panels is obtained by evaluating Eq. (13) at the measured panel temperatures and summing over all active panels. It should be noted that the panel contribution is not represented by an idealized thermal-output assumption. Instead, the reported panel term corresponds to the measured electrical input required to maintain the observed panel temperatures under the fixed bench boundary conditions and therefore reflects the effective bench-specific losses implicitly contained in the fitted coefficients.

Table 6
Coefficients for estimating the electrical power of the radiant heating panels as a function of panel surface temperature T_i. The linear model $P_{\mathrm{el,panel},i}(T_i) = \beta_{0,i} + \beta_{1,i}T_i$ is based on current measurements on the climate bench [7,33].

panel ID	Position	$\beta_{0,i}$ [W]	$\beta_{1,i}$ [W/K]
1	Rear window	542.79	−2.13
2	Side window	848.57	−2.83
3	Door panel	394.09	−1.21
4	Center console	516.86	−1.53
5	Headliner	567.81	−1.83
6	Windscreen	832.10	−1.51
7	Instrument-panel (lower)	262.80	−0.85
8	Instrument-panel (upper)	540.25	−1.35
9	Footwell	540.25	−1.35

5.7.3. Total HVAC electrical power and coefficient of performance

In battery-electric vehicles, the thermal load generated by the HVAC system is typically provided either by a PTC auxiliary heater or by a vapor-compression heat pump. In heating mode, the coefficient of performance is defined as

$$\mathrm{COP}(T_{\mathrm{amb}}) = \frac{\dot{Q}_{\mathrm{heat}}}{P_{\mathrm{el,HP}}}, \tag{14}$$

where $P_{\mathrm{el,HP}}$ is the electrical input power to the heat pump and $\dot{Q}_{\mathrm{heat}}$ is the delivered heating capacity. In cooling mode, the analogous efficiency metric is the energy efficiency ratio $\mathrm{EER} = \dot{Q}_{\mathrm{cool}}/P_{\mathrm{el,HP}}$.

For compact notation, the symbol $\eta(T_{\mathrm{amb}})$ is used as the scenario-specific efficiency factor, where $\eta = \mathrm{COP}$ in heating mode and $\eta = \mathrm{EER}$ in cooling mode. The total electrical HVAC power for a stationary operating point is then estimated as

$$P_{\mathrm{el,HVAC}} = \frac{\dot{Q}_{\mathrm{heat}} + \dot{Q}_{\mathrm{cool}}}{\eta(T_{\mathrm{amb}})} + \sum_{i=1}^{N_{\mathrm{panel}}} P_{\mathrm{el,panel},i}(T_i). \tag{15}$$

This model provides a consistent engineering estimate of total HVAC electrical power across all operating points. The scenario-specific COP and EER assumptions are used to compare relative energy demand across winter, transitional, and summer conditions. They are not intended to replace a full vehicle-level thermal or energy simulation. The resulting electrical-power values should therefore be interpreted as comparative engineering estimates for the investigated stationary operating space. They support relative comparisons between scenarios and actuator strategies, but they do not replace a full vehicle-level simulation with operating-point-dependent heat-pump maps, transient battery interaction, and road-load coupling.

6. Results

This section presents the main findings of the steady-state climate-chamber study and the associated energy assessment. The results are structured to first highlight the scenario-dependent comfort–energy trade-off of the hybrid convective–radiant HVAC concept and the resulting actuator-prioritization rules. The predictive performance of the forward surrogate models is then reported as methodological support for the underlying setpoint search. Unless stated otherwise, the reported validation settings correspond to the enveloping air-distribution concept, which provided the most robust overall comfort performance across the investigated operating space. In practical terms, this repeated selection indicates that the enveloping concept offered the broadest set of comfort-feasible candidates across scenarios. Compared with more directly impinging airflow patterns, it reduced the risk of locally excessive upper-body exposure while still allowing sufficient thermal support of distal and lower-body regions through the combined action of convection and radiation.

Table 7
Optimized HVAC setpoints used for the evaluated validation operating points in three ambient scenarios: winter (−10 °C), transitional (+16 °C) and summer (+28 °C), reported for driver and relax seating positions. For +16 °C, two operating modes are listed: (i) hybrid operation with explicit radiant-panel setpoints and (ii) convection-only operation with radiant heating deactivated. For +28 °C, radiant heating is deactivated and only convective setpoints are reported.

Setting	−10 °C		+16 °C		+28 °C	
	Driver	Relax	Driver	Relax	Driver	Relax
Hybrid mode (radiant setpoints active)						
Air-distribution concept [–]	enveloping	enveloping	enveloping	enveloping	–	–
Outlet air temperature T_{out} [°C]	31	31	23	26	–	–
Panel temperature console [°C]	31	40	32	29	–	–
Panel temperature door [°C]	36	38	34	31	–	–
Panel temperature footwell [°C]	50	50	30	30	–	–
Fan speed n_{fan} [rpm]	1728	1821	1800	1800	–	–
Convection-only mode (radiant off)						
Air-distribution concept [–]	–	–	enveloping	enveloping	enveloping	enveloping
Outlet air temperature T_{out} [°C]	–	–	26	27	21	21
Mean panel temperature T_{IR} [°C]	–	–	off	off	off	off
Fan speed n_{fan} [rpm]	–	–	959	920	1671	1709

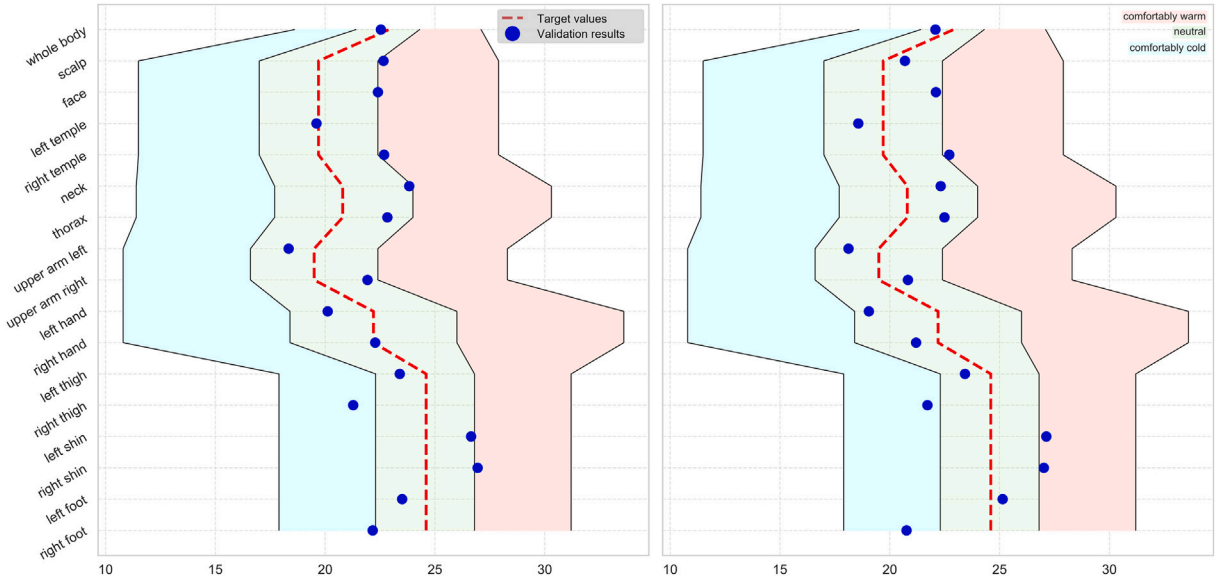

Fig. 7. Validation results for the winter scenario at −10 °C ambient temperature for driver (left) and relax (right) seating positions using the enveloping air-distribution concept. Points indicate measured steady-state equivalent temperatures of the sixteen body segments; shaded areas denote the neutral comfort ranges according to Nilsson for the respective segments.

6.1. Scenario-based validation of thermal comfort

For each ambient scenario, the surrogate-based search identifies actuator settings that keep the segmental equivalent temperatures of the climate dummy as close as possible to the Nilsson neutral zone while minimizing electrical HVAC power. When no fully feasible operating point exists within the discrete measurement grid, the selected setting minimizes the largest remaining local deviation from the neutral bands, so that no strongly under- or overheated body region is masked by otherwise neutral segments. The selected operating points are then validated by the corresponding steady-state measurements.

6.1.1. Winter scenario: −10 °C

Table 7 summarizes the optimized HVAC settings for the winter scenario. For both seating configurations, the enveloping air-distribution concept is selected. The outlet air temperature remains at a moderate level, while comparatively high radiant-panel temperatures are used to support lower-body and torso comfort without excessively increasing the mixed-air temperature.

In the relax position, the unconstrained optimum suggests comparatively high center-console panel temperatures, which would shift the right thigh segment above its neutral band. In the evaluated validation setting, the center-console panel was therefore limited to approximately 40 °C, while the remaining radiant panels and the convective setpoints were kept at the optimized values. This local restriction slightly reduces equivalent temperature at the upper legs but preserves near-neutral comfort across the remaining segments.

Fig. 7 shows the measured steady-state equivalent temperatures for both seating configurations at −10 °C. For each of the sixteen body segments, the points represent stationary t_{eq} values and the shaded bands indicate the corresponding Nilsson neutral ranges. For both driver and relax posture, the majority of segments lie within or very close to the neutral zone. Slight underheating appears mainly at exposed extremities such as feet and hands, whereas no segment enters the “too warm” region. The comparison with the neutral bands confirms that the optimized operating points achieve near-neutral local comfort for both seating positions in cold conditions within the investigated grid.

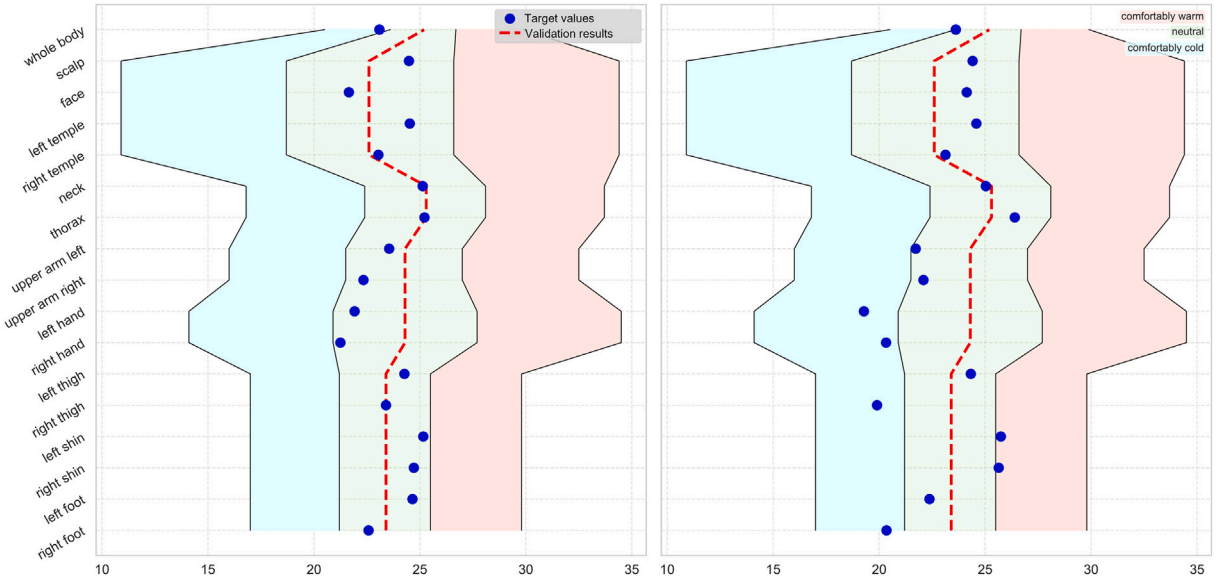

Fig. 8. Measured segmental equivalent temperatures in the summer validation scenario at +28 °C for driver and relax seating positions using the enveloping air-distribution concept. Upper-body segments are maintained near neutral or slightly cool conditions.

6.1.2. *Summer scenario:* +28 °C

In the summer scenario, radiant heating is deactivated and the optimization selects convection-only settings that balance cooling intensity against draft risk. The optimized actuator values are listed in Table 7. Again, the enveloping air-distribution concept is selected, together with moderately cool outlet temperatures and fan speeds.

The measured equivalent temperatures for these settings are shown in Fig. 8. For both seating positions, upper-body segments are kept in the neutral or slightly cool range, while lower-body segments remain somewhat warmer. This is consistent with the target of a slightly cooler sensation at head and torso in warm environments. Extremities such as head and hands show somewhat larger deviations from neutrality but remain within acceptable comfort limits for the investigated steady-state conditions without solar gains.

6.1.3. *Transitional scenario:* +16 °C

At +16 °C, the comfort–energy trade-off changes qualitatively. Both hybrid convective–radiant and convection-only solutions are feasible within the investigated grid, and Table 7 therefore lists both operating modes. Fig. 9 compares the measured equivalent temperatures for the hybrid and convection-only settings.

The hybrid configuration yields slightly higher equivalent temperatures in some lower-body segments, but both operating modes remain within acceptable comfort ranges. The segmental comfort differences are therefore small. From a control perspective, this scenario forms a break-even region in which radiation no longer provides a commensurate comfort benefit.

6.2. *Electrical power demand and range impact*

The electrical power demand of the HVAC system is evaluated for the optimized neutral-comfort configurations in the three ambient scenarios. For each configuration, the required thermal power of the convective system and the radiant panels is combined with scenario-specific coefficients of performance to obtain the corresponding electrical power and the resulting WLTP range for the reference cycle. Consistent with the underlying vehicle and heat-pump model, COP or EER values of 2.3, 2.7, and 3.5 are used for ambient temperatures of −10 °C, +16 °C, and +28 °C, respectively. For the resistive radiant panels, electrical input power is used consistently as the energy-relevant quantity for the range assessment. The effective heat gain to the cabin depends on radiative exchange and thermal losses. Even if the absolute range values depend on the assumed scenario-specific efficiency factors, the qualitative conclusion is unchanged within the present dataset: around +16 °C, additional radiant activation causes a clear electrical-power penalty while producing only marginal comfort gains.

6.2.1. *Winter and summer scenarios*

Table 8 summarizes the thermal powers, electrical HVAC power, and resulting WLTP range for the winter and summer validation configurations. At −10 °C, the hybrid architecture combines substantial convective thermal power with additional radiant input. The total electrical HVAC power lies between 3.60 and 3.84 kW, leading to WLTP ranges of 63.40 and 64.78 km for driver and relax posture, respectively.

At +28 °C, radiant panels are inactive and only convective cooling is used. The higher cooling efficiency reduces the electrical power demand to 0.53 and 0.60 kW, yielding WLTP ranges of 88.29 and 87.57 km. Comparing winter heating and summer cooling, more than six times as much electrical power is required at −10 °C to maintain neutral comfort than at +28 °C. This contrast is conservative for summer operation because the present climate-chamber conditions exclude solar gains.

6.2.2. *Transitional scenario:* +16 °C

At +16 °C, the energy–comfort trade-off becomes the dominant engineering result of the study. For both seating positions, neutral thermal comfort can be achieved with and without active radiant panels. However, the energy demand differs strongly between the two modes.

For the driver position, the convection-only configuration requires a convective thermal power of 1.37 kW and an electrical HVAC power of 0.51 kW, resulting in a WLTP range of 88.50 km. The hybrid configuration increases the convective thermal power to 1.98 kW and adds 1.32 kW of electrical radiant power, leading to a total electrical HVAC power of 2.05 kW and a WLTP range of 74.81 km. For the relax position, the same pattern is observed: convection-only operation yields 0.50 kW total HVAC electrical power and 88.61 km WLTP range, whereas the hybrid mode yields 2.17 kW and 73.91 km, respectively.

Thus, activating radiant heating at +16 °C increases the electrical HVAC power from roughly 0.5 kW to roughly 2.1 kW for both postures and causes a WLTP range penalty on the order of 15–17%, while

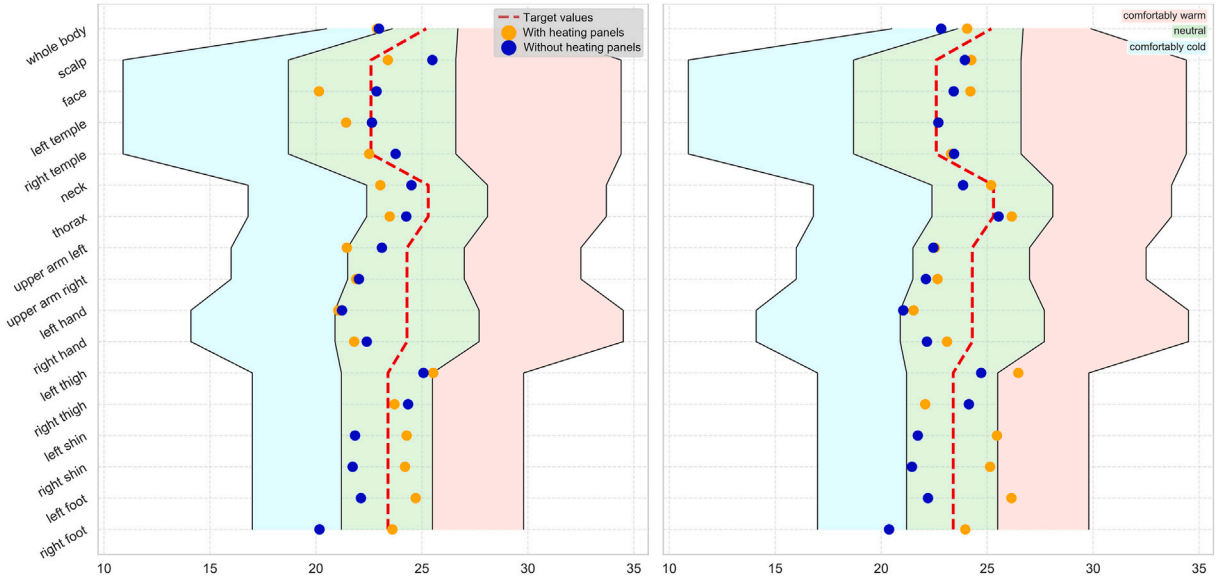

Fig. 9. Measured segmental equivalent temperatures at +16 °C ambient temperature for hybrid convective–radiant and convection-only settings in driver and relax seating positions using the enveloping air-distribution concept. Both modes achieve acceptable comfort, with only minor differences between segments.

Table 8
Thermal powers, electrical HVAC power and resulting WLTP range for neutral thermal comfort in the winter (−10 °C) and summer (+28 °C) validation scenarios.

Scenario	Seat	$P_{th,conv}$ [kW]	$P_{th,IR}$ [kW]	COP [–]	$P_{el,conv}$ [kW]	$P_{el,IR}$ [kW]	Range [km]
Winter −10 °C	Driver	5.87	1.29	2.3	2.55	1.29	63.40
Winter −10 °C	Relax	6.37	0.82	2.3	2.77	0.82	64.78
Summer +28 °C	Driver	1.87	0.00	3.5	0.53	0.00	88.29
Summer +28 °C	Relax	2.11	0.00	3.5	0.60	0.00	87.57

Table 9
Pooled intra-scenario cross-validation performance for forward prediction of the sixteen stationary segmental equivalent temperatures t_{eq} from scenario, posture, air-distribution concept, and actuator setpoints. Range/mean values summarize variability and overall performance across folds, scenarios, and body segments.

Model	R^2 (range / mean)	MAE [K] (range / mean)
XGBoost	0.96–0.99 / 0.978	0.71–1.04 / 0.856
Random Forest	0.92–0.97 / 0.949	1.11–1.93 / 1.411
Linear regression (baseline)	0.74–0.93 / 0.872	1.81–3.05 / 2.248

the measured segmental comfort differences remain small. This identifies +16 °C as a transitional break-even region in which convection alone is already sufficient to achieve near-neutral comfort. From an actuator-prioritization perspective, radiant heating should therefore be reserved for clearly cold conditions and suppressed once neutral comfort is reachable by convection.

6.3. Surrogate-model accuracy and robustness

The following results quantify the predictive accuracy of the forward surrogate models for the sixteen segmental equivalent temperatures t_{eq} and delimit their domain of validity. These metrics do not constitute the primary engineering result of the study, but they provide methodological support for the surrogate-based search described above.

6.3.1. Pooled intra-scenario cross-validation (interpolation)

Table 9 reports pooled intra-scenario 5-fold cross-validation results for predicting the sixteen steady-state segmental equivalent temperatures. The XGBoost surrogate achieves the highest interpolation accuracy, with R^2 values in the range 0.96–0.99 and MAE between 0.71 and 1.04 K, corresponding to a mean R^2 of 0.978 and a mean MAE of 0.856 K. Random Forest provides slightly lower accuracy, with mean $R^2 = 0.949$ and mean MAE = 1.411 K. The linear regression baseline remains competitive but clearly inferior to the tree-based ensembles, with mean $R^2 = 0.872$ and mean MAE = 2.248 K. The baseline result indicates that a substantial fraction of the mapping is approximately linear, whereas non-linear interactions are required for sub-Kelvin surrogate accuracy.

The use of ensemble-based surrogate models should be interpreted against the specific requirements of the comfort-constrained setpoint search rather than against large-data predictive modeling in general. The underlying task is to approximate a mixed discrete–continuous mapping from ambient scenario, seating posture, air-distribution concept, and multiple continuous actuator settings to sixteen coupled segmental equivalent-temperature responses. Simple grid interpolation is of limited practical value in this setting because the operating space combines categorical mode changes with non-linear actuator interactions across body regions. The linear regression baseline confirms that a substantial share of the mapping is approximately linear, but its mean absolute error of 2.248 K approaches the width of the Nilsson neutrality bands, which are typically 3–5 K wide per segment. At this error level, a significant fraction of candidate operating points would be misclassified as comfort-feasible or infeasible during the constrained search. The XGBoost surrogate reduces this error to 0.856 K and thereby provides the prediction headroom required for reliable segment-level constraint checking across sixteen simultaneous targets. Machine learning is therefore employed here as a compact non-linear surrogate for fast screening of candidate operating points within the measured space, not as a claim of superior extrapolation beyond it.

6.3.2. Stress tests: input-noise sensitivity and leave-one-scenario-out extrapolation

To bound sensitivity to perturbed inputs, Gaussian noise with σ = 1 K is injected into the continuous inputs in original feature space before preprocessing, and the increase in MAE is evaluated across Monte-Carlo trials. Random Forest shows the strongest robustness with $\Delta MAE_{mean} = 0.633$ K (sd 0.104 K), followed by the linear baseline with

ΔMAE_{mean} = 1.626 K and XGBoost with ΔMAE_{mean} = 1.977 K. This reveals a clear trade-off: XGBoost yields the lowest interpolation error, whereas Random Forest is least sensitive to input perturbations.

A leave-one-scenario-out evaluation is used as a controlled extrapolation stress test across climate conditions. When one ambient scenario is withheld entirely during training, the performance drops markedly. XGBoost reaches R^2_{mean} = 0.318 and MAE_{mean} = 4.043 K, Random Forest reaches R^2_{mean} = 0.239 and MAE_{mean} = 4.369 K, and the linear baseline reaches R^2_{mean} = −0.143 and MAE_{mean} = 4.939 K. The surrogate models are therefore reliable for interpolation within the measured operating space, but genuine scenario extrapolation remains limited and is treated as a scope limitation of the present dataset.

7. Discussion

This section interprets the experimental and modeling results with regard to thermal comfort and electrical HVAC power in hybrid convective–radiant systems for Level-4 battery-electric vehicles. The main emphasis is placed on the scenario-dependent comfort–energy trade-off and the resulting actuator-prioritization rules. The role of the forward surrogate is then discussed as a methodological enabler for steady-state setpoint selection within the measured operating space. Finally, implications, limitations, and directions for future work are outlined.

7.1. Energy–comfort trade-offs across ambient scenarios

The results show that the comfort–energy relationship of the investigated hybrid HVAC architecture is strongly scenario dependent. In the winter case at −10 °C, the combination of convection and infrared radiation reduces underheating in distal body regions and supports a more homogeneous segmental equivalent-temperature distribution without requiring excessively high convective outlet temperatures. This behavior is physically plausible because radiant heating can compensate for cold surrounding surfaces and stratification effects, especially in lower-body regions, and is consistent with previous work on radiant and contact-related comfort concepts in cold vehicle environments [4,51,53]. In energy terms, the corresponding hybrid operating points require about 3.6–3.8 kW electrical HVAC power and reduce the WLTP range to approximately 63–65 km in the investigated reference cycle (Table 8). The strong winter penalty relative to summer operation reflects the well-known dominance of heating loads in battery-electric vehicles under cold ambient conditions [25].

The sensitivity of these estimates to the assumed COP values can be bounded qualitatively. If the winter COP were varied from the assumed 2.3 to a plausible range of 1.8–2.8, the convective electrical power would change by approximately ±15–20% relative to the reported values, shifting the estimated WLTP range by a corresponding margin. The qualitative conclusion that winter hybrid operation requires several times the electrical power of summer convection-only cooling remains robust across this range. At +16 °C, the dominant energy penalty arises from the resistive radiant panels, whose electrical input power is measured directly and does not depend on the COP assumption. Even a substantial COP variation at +16 °C therefore does not alter the finding that hybrid operation approximately quadruples the electrical HVAC power demand relative to convection-only operation. The reported energy comparisons should be interpreted as order-of-magnitude engineering estimates whose relative ranking across scenarios and operating modes is stable, even though the absolute values depend on the specific COP assumptions.

At +16 °C, the trade-off changes qualitatively and yields the strongest practical design finding of the study. In this transitional regime, convection - only operation already achieves near-neutral segmental equivalent temperatures, whereas additional radiant activation increases electrical HVAC power substantially without producing a commensurate comfort benefit (Fig. 9). The quantitative comparison shows that the convection-only mode requires only about 0.5 kW electrical HVAC power, whereas the hybrid mode requires about 2.1 kW, corresponding to a WLTP range penalty on the order of 15–17% for both seating positions. The transitional case therefore acts as a break-even region in which hybrid operation becomes energetically unfavorable despite acceptable comfort in both modes. This result is particularly important because it shows that radiant heating is not a universally beneficial comfort actuator. Instead, it should be actively suppressed once neutral comfort is already reachable by convection.

In the summer scenario at +28 °C, radiant panels remain inactive and the relevant control levers are outlet-air temperature, blower speed, and air-distribution concept. The optimized configurations keep upper-body segments slightly cool and lower-body segments closer to neutral (Fig. 8), which is consistent with reported preferences for stronger cooling at the face and upper torso in warm environments [3,66]. The electrical HVAC power of about 0.5–0.6 kW yields WLTP ranges of approximately 87–88 km in the investigated reference cycle (Table 8). Because the climate-chamber setup does not include solar gains, this summer assessment is conservative and likely underestimates real-world cooling demand [66].

Taken together, the scenario comparison shows that hybrid HVAC architectures should not be interpreted as uniformly advantageous across all operating conditions. In clearly cold environments, radiant elements are an effective complement to convection, especially for lower-body comfort. In moderate environments, convection-only operation is energetically preferable once acceptable comfort has been reached. In warm environments, radiant elements are unnecessary and the design space is dominated by convective cooling and draft management.

7.2. Selective use of radiant heating and actuator prioritization

Across scenarios, the results support a clear actuator-prioritization rule set. Radiant heating is most useful in clearly cold conditions, where it can selectively raise lower-body t_{eq} levels that are difficult to stabilize with convection alone without causing upper-body overheating. This is especially relevant for feet, lower legs, and adjacent torso regions, where purely convective heating often remains limited by stratification and comfort constraints at the head.

At +16 °C, the energetic cost of radiant actuation dominates because convection alone already provides near-neutral conditions. Radiant heating should therefore be treated as a winter-focused actuator and should be deactivated in transitional and warm conditions unless specific boundary conditions, such as severe cold-surface asymmetry or limited convective capacity, make local radiant support necessary.

The bench geometry also indicates that the placement and zoning of radiant elements matter at least as much as their activation. Panels addressing the lower body, such as the footwell and lower lateral regions, contribute most directly to mitigating distal underheating. In contrast, strong radiation into upper cabin regions can shift the head and upper torso toward overheating. The present findings therefore support a design strategy that concentrates radiant support on lower-body regions while using convective flow shaping to avoid hot-air accumulation near the head [48,49].

7.3. Interpretation of the forward surrogate framework

From a modeling perspective, the present framework is best interpreted as a forward surrogate for steady-state setpoint evaluation. The model predicts the sixteen stationary segmental equivalent temperatures from scenario descriptors and actuator settings and thereby allows candidate operating points to be screened rapidly against local comfort constraints. This is useful for control-oriented analysis because a large number of feasible and infeasible candidates can be evaluated without repeated climate-chamber measurements.

A hierarchical classification-based formulation was initially considered because the three air-distribution concepts represent physically distinct flow modes. For the final manuscript, however, the problem was simplified to a direct forward-surrogate formulation in which the

air-distribution concept is retained as a discrete operating variable and evaluated by direct enumeration within the constrained setpoint search. This avoids additional classifier complexity for the present steady-state interpolation task while preserving the physically distinct operating concepts.

Within the represented operating space, the surrogate performs strongly (Table 9). The cross-validation results confirm that a substantial part of the mapping is approximately linear, but non-linear interactions are required for sub-Kelvin accuracy.

At the same time, the robustness analyses clarify the model's scope. The Monte-Carlo input-noise test shows that Random Forest is least sensitive to perturbed inputs, whereas XGBoost is more accurate but also more noise-sensitive. More importantly, the leave-one-scenario-out stress test reported in Section 6.3 shows a pronounced drop in performance when an entire ambient scenario is withheld during training. The surrogate should therefore be interpreted primarily as an interpolation model within the measured scenario space rather than as a general climate-extrapolation model. This does not invalidate the present study, but it limits the domain of application and implies that deployment to additional climates requires explicit data coverage, targeted retraining, or additional physics-based constraints.

The main methodological value of the surrogate is therefore not that it replaces physical understanding, but that it makes the experimentally observed comfort landscape computationally accessible. It enables systematic screening of discrete operating concepts and continuous actuator settings under segment-level comfort constraints and thereby supports engineering decisions about when hybrid operation is justified and when it is not.

7.4. Implications for HVAC setpoint selection in level-4 electric vehicles

The combination of hybrid hardware, segmented equivalent - temperature measurement, and surrogate-based evaluation has direct implications for HVAC design and operation in Level-4 battery-electric cabins. First, the results show that comfort targets defined by segmented t_{eq} are practically attainable in a repeatable bench environment with a limited actuator set, which supports DIN EN ISO 14,505–2 as a useful engineering reference for non-uniform automated cabins [14]. The present work should therefore not be understood as proposing a validated cabin controller but as providing a structured engineering basis for identifying preferred steady-state operating regions and actuator combinations.

Second, the results suggest a scenario-dependent setpoint-selection logic rather than a generic comfort-maximization strategy. Ambient condition and use case should first delimit the admissible mode space, for example by deciding whether radiant support is necessary at all. Within that restricted operating space, actuator settings can then be selected by evaluating candidate points with the forward surrogate and minimizing electrical HVAC power subject to segment-level comfort constraints. In this sense, the work supports discrete mode selection combined with constrained setpoint search, rather than a broadly generalized real-time control claim.

In a practical implementation, the present surrogate would most naturally serve as a supervisory steady-state layer within a hierarchical control architecture. Such an architecture would use the surrogate to preselect admissible operating modes and to initialize energy-aware setpoints, while dedicated lower-level controllers handle transient HVAC dynamics, actuator tracking, and battery constraints. Outside quasi-steady phases or outside the experimentally covered domain, fallback logic or physics-based models would remain necessary.

Third, lower-body comfort emerges as a key driver of radiant usefulness in cold conditions. This is especially relevant for Level-4 cabins because more relaxed postures and non-driving-related use cases alter body posture and exposure patterns compared with conventional driver-focused seating [23,42,63]. The present results therefore connect the Level-4 use case not merely to a different seat geometry, but to a different thermal-control priority structure in which local non-uniformity becomes more important than in conventional driver-focused cabins.

7.5. Methodological considerations and limitations

The conclusions of the present study are bounded by the experimental scope, the dataset structure, and the modeling assumptions.

- **Steady-state scope.** The dataset consists of quasi-steady climate-chamber operating points and does not represent entry transients, pull-down, warm-up, solar load build-up, or rapidly changing boundary conditions. The present framework should therefore be interpreted as a steady-state sizing and setpoint-selection tool within the measured operating space, not as a validated real-time cabin controller for arbitrary driving situations [3,33].
- **Restricted climate coverage and extrapolation limits.** Only three fixed ambient scenarios and two seating postures are covered. As shown by the leave-one-scenario-out stress test, scenario-level extrapolation to unseen climates remains limited. The surrogate is therefore reliable primarily within the represented operating space, while broader deployment requires additional experimental coverage or model adaptation.
- **Occupant realism and subjective validation.** The climate dummy represents one 50th-percentile male geometry with fixed clothing and constant metabolic assumptions. It provides an objective and spatially resolved comfort-oriented engineering reference, but unlike real occupants it does not reproduce human thermophysiological regulation [16,18,45]. In Level-4 use cases, this limitation is compounded by posture shifts and changing usage patterns that alter body posture and exposure conditions [23,63]. Real occupants exhibit thermoregulatory responses, behavioral adaptation, and inter-individual variability in subjective perception that the constant-temperature manikin cannot replicate. Prior studies have shown that manikin-based equivalent temperatures correlate well with group-mean thermal sensation under controlled conditions, but individual responses can deviate substantially. The present results should therefore not be interpreted as a substitute for human-subject validation but as identifying comfort-feasible operating points in an objective benchmark sense, whereas occupant-facing comfort claims require dedicated human-subject data.
- **Solar radiation and additional real-world boundary conditions.** Solar gains, glazing asymmetries, and systematically varied humidity or latent loads are not included as independent design variables in the experimental design. In real cabins, solar radiation and glazing effects can substantially alter mean radiant temperature fields and cooling demand [66]. The transfer of the reported summer findings to sun-exposed vehicle operation should therefore be made with caution.
- **Seat contact and conductive heat transfer.** The comfort assessment is based on equivalent temperature according to DIN EN ISO 14,505–2 and therefore focuses on convective and radiative heat exchange. Conductive heat transfer at seat contact regions is not modeled as an active control path in the present concept and is not resolved separately as a control variable. This may affect local comfort interpretation in back and pelvis contact regions [58].
- **Simplified COP assumptions.** The energy model uses fixed scenario-specific COP and EER values rather than operating-point-dependent heat-pump efficiency maps. In real vehicle systems, compressor efficiency varies with refrigerant conditions, ambient temperature, and thermal load. The reported electrical-power and WLTP-range values are therefore valid for relative mode comparison within the present study but do not substitute for a full vehicle-level energy simulation with transient battery interaction and road-load coupling.

7.6. Outlook

A direct next step from a control perspective is not merely to increase predictive complexity but to embed the present steady-state surrogate into a hierarchical control architecture. In such an architecture, the surrogate would provide mode preselection and comfort-feasible setpoint candidates on a slower supervisory horizon, whereas transient thermal dynamics, actuator tracking, and disturbance rejection would be handled by dedicated dynamic controllers or physics-based predictive models. The present work provides the necessary offline component for such an architecture, while the online component remains to be developed.

A necessary further step is targeted human-subject validation under selected winter and transitional steady-state conditions to quantify how reliably the manikin-based neutrality criterion predicts subjective local and global comfort under combined convective–radiant operation. Such validation is particularly important for Level-4 scenarios, where posture, task, and passive exposure duration may systematically alter the relation between objective thermal state and perceived comfort. Combining the present objective framework with subjective human feedback and physiological proxies would also support hybrid objective–subjective comfort models for future cabin applications [6,22].

At the hardware level, the results already indicate that further optimization of radiant-panel placement and zoning, especially for lower-body support in cold conditions, is likely more valuable than broad activation of radiant elements across all climates.

8. Conclusion

This study developed and evaluated a data-driven steady-state setpoint-selection framework for a hybrid convective–radiant HVAC concept in a Level-4 battery-electric vehicle cabin. The contribution is not a general real-time HVAC control strategy but a scenario-specific engineering tool for identifying comfort-feasible operating points and actuator-prioritization rules within the experimentally represented operating space. Climate-chamber experiments were conducted in a vehicle-like front-cabin mock-up at three ambient temperatures (−10 °C, +16 °C, and +28 °C), two seating postures, and three air-distribution concepts. Local thermal conditions were quantified by segmental equivalent temperatures t_{eq} in sixteen body zones, mapped to the Nilsson comfort zones, and used to train forward surrogate models that predict stationary segmental t_{eq} values from scenario descriptors and actuator settings. The trained surrogate was then embedded in a constrained search over the admissible actuation space to identify comfort-feasible operating points with minimum electrical HVAC power.

- A structured steady-state dataset was generated across three ambient scenarios, two seating postures, and three air-distribution concepts, covering hybrid convective - radiant heating as well as convection-only operation. The dataset links actuator settings such as outlet-air temperature, fan speed, and radiant-panel temperatures to sixteen segmental t_{eq} responses and corresponding electrical HVAC power.
- Forward surrogate models based on Random Forest and XGBoost predicted the sixteen stationary segmental t_{eq} values with high accuracy in pooled intra-scenario cross-validation. XGBoost achieved a mean $R^2 = 0.978$ and a mean MAE = 0.856 K, outperforming Random Forest ($R^2 = 0.949$, MAE = 1.411 K) and a linear regression baseline ($R^2 = 0.872$, MAE = 2.248 K). The leave-one-scenario-out stress test showed a pronounced loss in extrapolation performance, indicating that the surrogate is reliable primarily for interpolation within the represented operating space. Monte-Carlo input perturbations further showed a trade-off between accuracy and robustness, with Random Forest being least sensitive to input noise.
- Comfort-feasible and energy-minimal operating points were derived and validated experimentally for winter, transitional, and summer conditions as well as for both seating postures. At −10 °C, hybrid operation with enveloping air distribution, moderate outlet-air temperature, and elevated radiant-panel temperatures achieved near-neutral segmental conditions for most body zones, with remaining deviations mainly at exposed extremities. At +28 °C, convection-only cooling maintained neutral or slightly cool upper-body conditions without activating radiant panels. At +16 °C, both convection-only and hybrid solutions remained within acceptable comfort bands, with only minor segmental differences between modes.
- The strongest practical result of the study is the scenario-dependent actuator prioritization. In winter, radiant support is beneficial because it helps stabilize lower-body and torso comfort without excessive convective heating. In summer, radiant actuation is unnecessary. In transitional conditions at +16 °C, activating radiant heating increased electrical HVAC power from roughly 0.5 kW in convection-only operation to roughly 2.1 kW in hybrid operation for both postures, causing a WLTP range penalty on the order of 15–17% while yielding only marginal comfort improvement. This identifies a clear break-even region in which radiant heating becomes energetically unfavorable and should be suppressed. From an implementation perspective, the present surrogate is most suitable as a supervisory decision-support layer for mode selection and setpoint initialization within future dynamic HVAC control architectures.
- Taken together, the results show that hybrid HVAC systems in Level-4 battery-electric cabins should be operated selectively rather than uniformly. Radiant actuation should be reserved for clearly cold conditions, especially to support lower-body comfort, whereas convection-only operation is preferable in mild and warm conditions once acceptable segment-level comfort has been achieved. The present contribution should accordingly be interpreted as a steady-state engineering basis for comfort-constrained mode selection and setpoint definition, and the reported comfort-feasible operating points remain objective engineering results that require confirmation by human-subject data before broader occupant-comfort claims can be made.

CRediT authorship contribution statement

Manuel Kipp: Writing – review & editing, Writing – original draft, Visualization, Validation, Supervision, Software, Resources, Project administration, Methodology, Investigation, Formal analysis, Data curation, Conceptualization. **Ruya Wang:** Writing – review & editing, Visualization, Validation, Software, Methodology, Investigation, Formal analysis, Data curation, Conceptualization. **Daniel Schmeling:** Writing – review & editing, Visualization, Formal analysis. **Yijie Sheng:** Writing – review & editing. **Klaus Bengler:** Writing – review & editing, Supervision.

Declaration of competing interest

The authors declare that they have no known competing financial interests or personal relationships that could have appeared to influence the work reported in this paper.

Acknowledgements

We would like to thank AUDI AG for generously providing the climate dummy and the outlet system for our research.

Data availability

The authors do not have permission to share data.

References

[1] H. Abdi, Partial least squares (PLS) regression, Encyclopedia for research methods for the social sciences 6 (2003) 7.

[2] M.A. Al Faruque, K. Vatanparvar, Modeling, analysis, and optimization of electric vehicle HVAC systems, in: 2016 21st Asia and South Pacific Design Automation Conference (ASP-DAC), IEEE, Macao, Macao, 2016, pp. 423–428, https://doi.org/10.1109/ASPDAC.2016.7428048, http://ieeexplore.ieee.org/document/7428048/.

[3] A. Alahmer, A. Mayyas, A.A. Mayyas, M.A. Omar, D. Shan, Vehicular thermal comfort models; a comprehensive review, Appl. Therm. Eng. 31 (2011) 995–1002, https://doi.org/10.1016/j.applthermaleng.2010.12.004, https://linkinghub.elsevier.com/retrieve/pii/S135943111000520X.

[4] T. Bauml, D. Dvorak, A. Frohner, D. Simic, Simulation and measurement of an energy efficient infrared radiation heating of a full electric vehicle, in: 2014 IEEE Vehicle Power and Propulsion Conference (VPPC), IEEE, Coimbra, Portugal, 2014, pp. 1–6, https://doi.org/10.1109/VPPC.2014.7007129, https://ieeexplore.ieee.org/document/7007129/.

[5] S. Bellocchi, G. Leo Guizzi, M. Manno, M. Salvatori, A. Zaccagnini, Reversible heat pump HVAC system with regenerative heat exchanger for electric vehicles: analysis of its impact on driving range, Appl. Therm. Eng. 129 (2018) 290–305, https://doi.org/10.1016/j.applthermaleng.2017.10.020, https://linkinghub.elsevier.com/retrieve/pii/S1359431117338875.

[6] Y. Boutahri, A. Tilioua, Machine learning-based predictive model for thermal comfort and energy optimization in smart buildings, Results Eng. 22 (2024) 102148, https://doi.org/10.1016/j.rineng.2024.102148, https://linkinghub.elsevier.com/retrieve/pii/S259012302400402X.

[7] D. Bradaric, Automatisierung Eines Variablen Klimaprüfstandes, Masterarbeit, Technische Universität München, Garching, 2020.

[8] L. Breiman, Random forests, Mach. Learn. 45 (2001) 5–32, https://doi.org/10.1023/A:1010933404324

[9] J.E. Brooks, K.C. Parsons, An ergonomics investigation into human thermal comfort using an automobile seat heated with encapsulated carbonized fabric (ECF), Ergonomics 42 (1999) 661–673, https://doi.org/10.1080/001401399185379, https://www.tandfonline.com/doi/full/10.1080/001401399185379.

[10] P. Böckh, T. Wetzel, Wärmeübertragung, Springer Berlin Heidelberg, Berlin, Heidelberg, 2017, https://doi.org/10.1007/978-3-662-55480-7. http://link.springer.com/10.1007/978-3-662-55480-7.

[11] T. Chen, T. He, M. Benesty, V. Khotilovich, Y. Tang, H. Cho, K. Chen, R. Mitchell, I. Cano, T. Zhou, Xgboost: extreme gradient boosting. R package version 0.4-2, 2015, https://www.scirp.org/reference/referencespapers?referenceid=3758236.

[12] I. Cvok, B. Škugor, J. Deur, Control trajectory optimisation and optimal control of an electric vehicle HVAC system for favourable efficiency and thermal comfort, Optim. Eng. 22 (2021) 83–102, https://doi.org/10.1007/s11081-020-09515-w

[13] P. Danca, A. Vartires, A. Dogeanu, An overview of current methods for thermal comfort assessment in vehicle cabin, Energy Procedia 85 (2016) 162–169, https://doi.org/10.1016/j.egypro.2015.12.322, https://linkinghub.elsevier.com/retrieve/pii/S1876610215029872.

[14] DIN EN ISO, DIN EN ISO 14505-2 ergonomie DER thermischen umgebung beurteilung DER thermischen umgebung in fahrzeugen teil 2: bestimmung DER Äquivalenttemperatur (ISO 14505-2:2006); deutsche fassung EN ISO 14505-2:2006, 2007, https://doi.org/10.31030/9765403, https://www.dinmedia.de/de/-/-/92274990. number: 145050-2.

[15] DIN EN ISO, DIN EN ISO 7730 ergonomie DER thermischen umgebung analytische bestimmung und interpretation DER thermischen behaglichkeit durch berechnung des PMV- und des PPD-indexes und kriterien DER lokalen thermischen behaglichkeit (ISO 7730:2025); deutsche fassung EN ISO 7730:2025, 2025, https://doi.org/10.31030/9720035, https://www.dinmedia.de/de/-/-/89417255.

[16] J. Fan, Thermal Manikins and Modelling, The Hong Kong Polytechnic University, Hong Kong, 2006. OCLC: 76908216.

[17] P.O. Fanger, Thermal Comfort: Analysis and Applications in Environmental Engineering, Copenhagen: Danish Technical Press, 1970, http://archive.org/details/thermalcomfortan0000fang.

[18] R.B. Farrington, J.P. Rugh, D. Bharathan, R. Burke, Use of a Thermal Manikin to Evaluate Human Thermoregulatory Responses in Transient, Non-Uniform, Thermal Environments, 2004, https://doi.org/10.4271/2004-01-2345, 2004–01–2345. https://www.sae.org/content/2004-01-2345/.

[19] A. Frohner, D. Dvorak, T. Bäuml, D. Simic, Novel heating concept for full electric vehicles, e & i Elektrotechnik und Informationstechnik 132 (2015) 168–171, https://doi.org/10.1007/s00502-015-0293-6, http://link.springer.com/10.1007/s00502-015-0293-6.

[20] M. Gis, P. Wiõniowski, M. Bednarski, Efficiency of electric vehicle interior heating systems at low ambient temperatures, Open Eng. 11 (2021) 499–507, https://doi.org/10.1515/eng-2021-0052, https://www.degruyter.com/document/doi/10.1515/eng-2021-0052/html.

[21] A. Höskuldsson, PLS regression methods, J. Chemom. 2 (1988) 211–228, https://doi.org/10.1002/cem.1180020306, https://analyticalsciencejournals.onlinelibrary.wiley.com/doi/10.1002/cem.1180020306.

[22] F. Jazizadeh, W. Jung, Personalized thermal comfort inference using RGB video images for distributed HVAC control, Appl. Energy 220 (2018) 829–841, https://doi.org/10.1016/j.apenergy.2018.02.049, https://linkinghub.elsevier.com/retrieve/pii/S0306261918301740.

[23] S. Jorlöv, K. Bohman, A. Larsson, Seating positions and activities in highly automated cars – a qualitative study of future automated driving scenarios, in: Proceedings of the IRCOBI Conference 2017, Antwerp, Belgium, 2017, pp. 13–22, Paper No. IRC-17-11.

[24] Y.J. Ju, J.R. Lim, E.S. Jeon, Prediction of AI-based personal thermal comfort in a Car using Machine-Learning algorithm, Electronics 11 (2022) 340, https://doi.org/10.3390/electronics11030340, https://www.mdpi.com/2079-9292/11/3/340.

[25] K.R. Kambly, T.H. Bradley, Estimating the HVAC energy consumption of plug-in electric vehicles, J. Power Sources 259 (2014) 117–124, https://doi.org/10.1016/j.jpowsour.2014.02.033, https://linkinghub.elsevier.com/retrieve/pii/S037877531400216X.

[26] B.H. Kang, H.J. Lee, A review of recent research on automotive HVAC systems for EVs, Int. J. Air-Cond. Refrig. 25 (2017) 1730003, https://doi.org/10.1142/S2010132517300038, https://www.worldscientific.com/doi/abs/10.1142/S2010132517300038.

[27] M. Kipp, J. Jacobs, K. Bengler, An objective analysis of using infrared panels for thermal comfort assessments in a vehicle environment, IEEE Access 13 (2025) 199247–199266, https://doi.org/10.1109/ACCESS.2025.3626693, https://ieeexplore.ieee.org/document/11222640/.

[28] M. Kipp, R. Wang, K. Bengler, Optimizing thermal comfort in highly automated vehicles: an AI-based HVAC management approach with radiant panels for winter conditions, 2025, https://doi.org/10.2139/ssrn.5571117, https://papers.ssrn.com/abstract=5571117.

[29] M. Konz, N. Lemke, S. Försterling, M. Eghtessad, Spezifische anforderungen an das Heiz-Klimasystem elektromotorisch angetriebener fahrzeuge, FAT-Schriftenreihe, No. 233, 2011, 90 pp.

[30] P. Kosack, R.F. Konikkara, R. Teutsch, S. Hoffmann, Entwicklung und implementierung von infrarotheizungen für fahrzeugkabinen und deren messtechnische beurteilung bezüglich thermischer behaglichkeit, in: K. Berns, K. Dressler, R. Kalmar, N. Stephan, R. Teutsch, M. Thul (Eds.), Commercial Vehicle Technology 2020/2021, Springer Fachmedien, Wiesbaden, 2021, pp. 291–307, https://doi.org/10.1007/978-3-658-29717-6_20

[31] K. Kruppok, F. Claret, P. Neugebauer, R. Kriesten, E. Sax, Validation of a 5-zone-car-cabin model to predict the energy saving potentials of a battery electric vehicle's HVAC system, IOP Conf. Ser. Mater. Sci. Eng. 383 (2018) 012037, https://doi.org/10.1088/1757-899X/383/1/012037, https://iopscience.iop.org/article/10.1088/1757-899X/383/1/012037.

[32] A.L. Kun, S. Boll, A. Schmidt, Shifting gears: user interfaces in the age of autonomous driving, IEEE Pervasive Comput. 15 (2016) 32–38, https://doi.org/10.1109/MPRV.2016.14, http://ieeexplore.ieee.org/document/7389268/.

[33] L. Küchle, Objektive Analyse Innovativer Pkw-Klimatisierungskonzepte Behaglichkeits- Und Energieeffizienzbewertungen Konvektiver Und Strahlungsbasierter Systeme, Masterarbeit, Fakultät Für Maschinenwesen, Technische Universität München, Garching, 2021.

[34] A. Lahlou, F. Ossart, E. Boudard, F. Roy, M. Bakhouya, Optimal management of thermal comfort and driving range in electric vehicles, Energies 13 (2020) 4471, https://doi.org/10.3390/en13174471, https://www.mdpi.com/1996-1073/13/17/4471.

[35] Y. Lee, H. Lee, B.H. Kang, J.K. Kim, Machine learning-based personal thermal comfort model for electric vehicles with local infrared radiant warmers, J. Mech. Sci. Technol. 35 (2021) 3239–3247, https://doi.org/10.1007/s12206-021-0644-7, https://link.springer.com/10.1007/s12206-021-0644-7.

[36] C. Liu, Y. Zhang, T. Gao, J. Shi, J. Chen, T. Wang, L. Pan, Performance evaluation of propane heat pump system for electric vehicle in cold climate, Int. J. Refrig. 95 (2018) 51–60, https://doi.org/10.1016/j.ijrefrig.2018.08.020, https://linkinghub.elsevier.com/retrieve/pii/S0140700718303165.

[37] H. Mohd Yunus, H. Nasution, A. Abdul Aziz, K. Sumeru, A.A. Dahlan, The effect of ambient temperature on the performance of automotive Air-Conditioning system, Appl. Mech. Mater. 819 (2016) 221–225, https://www.scientific.net/AMM.819.221., doi:https://www.scientific.net/AMM.819.221.

[38] H. Nilsson, I. Holmér, M. Bohm, O. Norén, Equivalent Temperature and Thermal Sensation - Comparison with Subjective Responses, 1997.

[39] H.O. Nilsson, Comfort Climate Evaluation with Thermal Manikin Methods and Computer Simulation Models (Ph.D. thesis), Department of Civil and Architectural Engineering, Royal Institute of Technology, Stockholm, 2004, http://doi.wiley.com/10.1034/j.1600-0668.2003.01113.x.

[40] H. Oi, K. Yanagi, K. Tabata, Y. Tochihara, Effects of heated seat and foot heater on thermal comfort and heater energy consumption in vehicle, Ergonomics 54 (2011) 690–699, https://doi.org/10.1080/00140139.2011.595513, https://www.tandfonline.com/doi/full/10.1080/00140139.2011.595513.

[41] L. Pan, C. Liu, Z. Zhang, T. Wang, J. Shi, J. Chen, Energy-saving effect of utilizing recirculated air in electric vehicle air conditioning system, Int. J. Refrig. 102 (2019) 122–129, https://doi.org/10.1016/j.ijrefrig.2019.03.018, https://linkinghub.elsevier.com/retrieve/pii/S0140700719301173.

[42] S. Parida, S. Mallavarapu, S. Abanteriba, M. Franz, W. Gruener, Seating postures for autonomous driving secondary activities, in: Y.W. Chen, A. Zimmermann, R.J. Howlett, L.C. Jain (Eds.), Innovation in Medicine and Healthcare Systems, and Multimedia, vol. 145, Springer Singapore, Singapore, 2019, pp. 423–434, https://doi.org/10.1007/978-981-13-8566-7_39, http://link.springer.com/10.1007/978-981-13-8566-7_39. series Title: Smart Innovation, Systems and Technologies.

[43] J. Pokorny, J. Fiser, Market research and definition of procedure to comparison of comfort measuring systems for a vehicle cabin, FAT-Schriftenreihe No. 363, 2022, 60 pp.

[44] W. Polifke, J. Kopitz, Wärmeübertragung - Grundlagen, Analytische Und Numerische Methoden, vol. 2, Pearson Deutschland GmbH, 2009, https://elibrary.pearson.de/book/99.150005/9783863266707. publisher: Pearson Deutschland.

[45] J.I. Priego-Quesada, New advances in human thermophysiology, Life 12 (2022) 1261, https://doi.org/10.3390/life12081261, https://www.mdpi.com/2075-1729/12/8/1261.

[46] Z. Qavidel Fard, Z.S. Zomorodian, S.S. Korsavi, Application of machine learning in thermal comfort studies: a review of methods, performance and challenges, Energy Build. 256 (2022) 111771, https://doi.org/10.1016/j.enbuild.2021.111771, https://linkinghub.elsevier.com/retrieve/pii/S0378778821010550.

[47] D. Ramsey, A. Bouscayrol, L. Boulon, A. Vaudrey, Simulation of an Electric Vehicle to Study the Impact of Cabin Heating on the Driving Range, 2020, https://doi.org/10.1109/VTC2020-Spring48590.2020.9129169
[48] A. Rolle, B. Schmandt, C. Guinet, K. Bengler, How can the thermal sensation be objectively determined in order to analyse different vehicle air conditioning concepts? in: Windsor Conference, 2020.
[49] A.D. Rolle, Objektive Bewertung Des Thermischen Komforts Im PKW Entwicklung Von Methodiken Für Aktuelle Und Zukünftige Klimakonzepte (Ph.D. thesis), Technische Universität München, Garching, 2022.
[50] C. Rommelfanger, L. Fischer, J. Frisch, C. Van Treeck, Linearization of thermal equivalent temperature calculation for fast thermal comfort prediction, Energies 14 (2021) 5922, https://doi.org/10.3390/en14185922, https://www.mdpi.com/1996-1073/14/18/5922.
[51] H. Sasaki, D. Sakamoto, Cabin comfort improvement and heating energy reduction under cold-condition by using radiative heater, SAE Technical Paper, 2022, https://doi.org/10.4271/2022-01-0202, https://www.sae.org/publications/technical-papers/content/2022-01-0202/. number: 2022-01-0202 Place: Warrendale, PA.
[52] S. Schilling, K. Franke, P. Schutzeich, D. Hemkemeyer, Auslegung DER innenraumklimatisierung von elektrofahrzeugen mittels klimamesspuppe, ATZ - Automob. Z. 125 (2023) 18–23, https://doi.org/10.1007/s35148-023-1644-y
[53] C. Schmidt, D. Wölki, C. van Treeck, Definition einer Äquivalenten kontakttemperatur als bezugsgröße zur bewertung DER ergonomischen qualität von kontaktbasierten klimatisierungssystemen in fahrzeugen, FAT-Schriftenr. (2018) 133.
[54] G. Suck, C. Spengler, Lösungen für das wärmemanagement von batteriefahrzeugen, ATZ - Automob. Z. 116 (2014) 12–19, https://doi.org/10.1007/s35148-014-0443-x, https://link.springer.com/10.1007/s35148-014-0443-x.
[55] T. Suzuki, K. Ishii, Air Conditioning System for Electric Vehicle, Technical Report 960688. SAE Technical Paper, 1996, https://doi.org/10.4271/960688. https://legacy.sae.org/publications/technical-papers/content/960688/.
[56] W. Wachenfeld, H. Winner, J.C. Gerdes, B. Lenz, M. Maurer, S. Beiker, E. Fraedrich, T. Winkle, Use cases for autonomous driving, in: M. Maurer, J.C. Gerdes, B. Lenz, H. Winner (Eds.), Autonomous Driving, Springer Berlin Heidelberg, Berlin, Heidelberg, 2016, pp. 9–37, https://doi.org/10.1007/978-3-662-48847-8_2
[57] A. Warey, S. Kaushik, B. Khalighi, M. Cruse, G. Venkatesan, Data-driven prediction of vehicle cabin thermal comfort: using machine learning and high-fidelity simulation results, Int. J. Heat Mass Transf. 148 (2020) 119083, https://doi.org/10.1016/j.ijheatmasstransfer.2019.119083, https://linkinghub.elsevier.com/retrieve/pii/S0017931019336348.
[58] A. Warthmann, I. Kohri, Y. Ozeki, H. Nagano, C. Van Treeck, Equivalent contact temperature (ECT) for personal comfort assessment – analytical description and definition of comfort limits, Ergonomics 67 (2024) 207–224, https://doi.org/10.1080/00140139.2023.2219044
[59] M. Wehowski, J. Grünwald, C. Heneka, D. Neumeister, Thermoelektrische wärmepumpe für Lithium-Ionen-Batterien, ATZ - Automob. Z. 115 (2013) 900–905, https://doi.org/10.1007/s35148-013-0308-8
[60] A. Westhoff, C. Marggraf-Micheel, J. Maier, P. Goerke, D. Schiepel, Untersuchung zum thermischen komfort im pkw für den grenzbereich des luftzugempfindens, FAT-Schriftenr. (2021) 76.
[61] Y. Wu, H. Liu, B. Li, J. Jokisalo, R. Kosonen, Y. Cheng, W. Zhao, X. Yuan, Evaluation and modification of the weighting formulas for mean skin temperature of human body in winter conditions, Energy Build. 229 (2020) 110390, https://doi.org/10.1016/j.enbuild.2020.110390, https://linkinghub.elsevier.com/retrieve/pii/S0378778820315760.
[62] X. Xu, L. Zhao, Z. Yang, Prediction models of overall thermal sensation and comfort in vehicle cabin based on field experiments, Int. J. Automot. Technol. 26 (2025) 269–282, https://doi.org/10.1007/s12239-024-00147-y, https://link.springer.com/10.1007/s12239-024-00147-y.
[63] Y. Yang, J.N. Klinkner, K. Bengler, How will the driver sit in an automated vehicle? – the qualitative and quantitative descriptions of Non-Driving postures (NDPs) when Non-Driving-Related-Tasks (NDRTs) are conducted, in: S. Bagnara, R. Tartaglia, S. Albolino, T. Alexander, Y. Fujita (Eds.), Proceedings of the 20th Congress of the International Ergonomics Association (IEA 2018), vol. 823, Springer International Publishing, Cham, 2019, pp. 409–420, https://doi.org/10.1007/978-3-319-96074-6_44, http://link.springer.com/10.1007/978-3-319-96074-6_44. series Title: Advances in Intelligent Systems and Computing.
[64] C. Yu, B. Li, Y. Wu, B. Chen, R. Kosonen, S. Kilpelainen, H. Liu, Performances of machine learning algorithms for individual thermal comfort prediction based on data from professional and practical settings, J. Build. Eng. 61 (2022) 105278, https://doi.org/10.1016/j.jobe.2022.105278, https://linkinghub.elsevier.com/retrieve/pii/S2352710222012840.
[65] S. Yun, C. Chun, J. Kwak, J.S. Park, C. Kwon, S. Kim, S. Seo, Prediction of thermal comfort of female passengers in a vehicle based on an outdoor experiment, Energy Build. 248 (2021) 111161, https://doi.org/10.1016/j.enbuild.2021.111161, https://linkinghub.elsevier.com/retrieve/pii/S037877882100445X.
[66] Z. Zhang, J. Wang, X. Feng, L. Chang, Y. Chen, X. Wang, The solutions to electric vehicle air conditioning systems: a review, Renew. Sustain. Energy Rev. 91 (2018) 443–463, https://doi.org/10.1016/j.rser.2018.04.005, https://linkinghub.elsevier.com/retrieve/pii/S1364032118302144.